Journal Pre-proofs

Paleoenvironment and paleobiogeography of the Lower Cretaceous carbonate successions of northern Tethyan margin: Examples from Northeastern and Central Iran

Masoumeh Gheiasvand, Karl B. Föllmi, Gérard M. Stampfli, Christian Vérard, Valeria Luciani, Michele Morsilli

PII: S1367-9120(21)00090-0
DOI: https://doi.org/10.1016/j.jseaes.2021.104752
Reference: JAES 104752

To appear in: *Journal of Asian Earth Sciences*

Received Date: 6 October 2020
Revised Date: 18 March 2021
Accepted Date: 19 March 2021

Please cite this article as: Gheiasvand, M., Föllmi, K.B., Stampfli, G.M., Vérard, C., Luciani, V., Morsilli, M., Paleoenvironment and paleobiogeography of the Lower Cretaceous carbonate successions of northern Tethyan margin: Examples from Northeastern and Central Iran, *Journal of Asian Earth Sciences* (2021), doi: https://doi.org/10.1016/j.jseaes.2021.104752

Paleoenvironment and paleobiogeography of the Lower Cretaceous carbonate successions of northern Tethyan margin: Examples from Northeastern and Central Iran

Masoumeh Gheiasvand[1*], Karl B. Föllmi[2,†], Gérard M. Stampfli[2], Christian Vérard[3], Valeria Luciani[4], Michele Morsilli[4]

[1] Department of Geology, Faculty of Sciences, Ferdowsi University of Mashhad, Mashhad, Iran

[2] Institute of Earth Sciences, University of Lausanne, CH-1015 Lausanne, Switzerland

[3] Institute of Environmental Sciences, University of Geneva, Geneva, Switzerland

[4] Department of Physics and Earth Sciences, University of Ferrara, Via Saragat 1, I-44121, Ferrara, Italy

[*] Corresponding author. E-mail address: masoumehgheiasvand@gmail.com

[†] Deceased.

Abstract

Lower Cretaceous carbonate successions outcrop extensively along the northern Tethyan margin in the Kopet-Dagh (NE Iran) and Yazd Block (Central Iran). These carbonate units are not well constraint in terms of stratigraphic, sedimentological, geochemical, and paleobiogeographic view point. To improve our knowledge, a detailed multidisciplinary study has been presented on two roughly coeval stratigraphic units in the two different areas, and correlated with other tethyan carbonates. The two stratigraphic units (Taft and Tirgan formations) have been deposited along a carbonate shelf with microfacies associations ranging from the outer-shelf to the inner-shelf settings. Diachrony in ages at the base and top of the stratigraphic units suggests the long-term subsidence effects during the Early

Cretaceous, followed by a Cimmerian phase of epi-orogenesis, and also the remnant paleoreliefs. New biostratigraphic data coupled with stable isotope $\delta^{13}C$ records show that the onset of carbonate production started much earlier than previously thought (Valanginian rather than Barremian). Our results also permit us to correlate the lower Aptian stratigraphic units with the OAE1a. The worldwide distribution of index microfossils including benthic foraminifera and colomiellids reported on paleobiogeographic reconstructions. They have been used to define paleobiogeographic provinces for the Valanginian, Hauterivian and Aptian intervals and show predominant basin connections. Significantly, the allochem content of the lithostratigraphic units and their phosphorus accumulation show phases of important heterozoan to photozoan carbonate production, which are recorded in other localities of the Tethyan realm as the consequence of global paleoceanographic changes.

Keywords: Early Cretaceous paleobiogeography; Benthic foraminifera; Phosphorus; Carbon isotope; Kopet-Dagh; Yazd Block.

1. Introduction

Lower Cretaceous successions are distributed worldwide along the northern and southern margins of the Tethys (e.g., Kilian, 1907; Jankičević, 1978; Afshar-Harb, 1979; Föllmi et al., 1994; Dini et al., 1998; Arnaud-Vanneau, 2006; Husinec and Sokač, 2006; Velić, 2007; Sudar et al., 2008; Masse et al., 2009a; Vasković et al., 2010; Godet et al., 2010, 2014; Morsilli et al., 2017; Schlagintweit, 2011; Stein et al., 2012; Picotti et al., 2019; Bonvallet et al., 2019; Gheiasvand et al., 2019, 2020; among others), the Pacific Ocean (e.g., Winterer et al., 1993; Arnaud-Vanneau and Silter, 1995; Ogg, 1995; Martin et al., 2004), and the Gulf of Mexico (e.g., González-León, 1994; Monreal and Longoria, 2000; González-León et al., 2008). These successions are usually located on the shallow-water platform and outer

shelf, beyond the platform margin, and record changes of nektonic (ammonites), planktonic, and benthic organisms (e.g., foraminifera, colomiellids, rudists, calcareous algae), which are useful as biostratigraphic indicators and for environmental reconstructions. Furthermore, fundamental changes in the carbonate factory of these successions, such as the switch from photozoan to heterozoan organisms, have been recorded. These changes relate to environmental variations, such as major global carbon cycle perturbations and a sea-level rise that lead to anoxic conditions in the world ocean (Schlanger and Jenkyns, 1976; Haq et al., 1987; Weissert et al., 1998; Westermann et al., 2010, 2013). The main methods of investigating changes in the oxygenation condition include stable isotope analysis, redox-sensitive trace-element distribution (e.g., U, Co, As, Cu, and Mn), phosphorus accumulation rates, and information on organic-matter (Föllmi et al., 2007; Stein, 2012; Westermann et al., 2013).

In Iran, Lower Cretaceous lithostratigraphic units of the southern and northern Neotethyan domains have been studied since the 1970s (e.g., Mehrnusch, 1973; Davoudzadeh, 1997; Bucur et al., 2012, 2013; Hosseini, 2014; Gheiasvand et al., 2020). In this research, successions of NE Iran (KD - Kopet-Dagh) and Central Iran (YB - Yazd Block) in the northern Tethyan domains (Stampfli and Borel, 2004; Wilmsen et al., 2009) are investigated. We present data from five stratigraphic sections of these areas through the Lower Cretaceous successions, with emphasis on the carbonate deposits from the Tirgan and Taft formations. Our study focuses on the following main objectives: 1) establishing the carbonate stable isotope records, and correlating them with the $\delta^{13}C$ values from a reference record to identify excursions and strengthen the calibration of the biostratigraphic records; 2) providing better constraints for the paleobiogeographic reconstructions of the Iranian Lower Cretaceous successions using benthic foraminifera and colomiellids; 3) recognising phases of important photozoan and heterozoan carbonate production using the phosphorus (P) content

and dominant groups of light-dependent and independent fauna; and finally 4) providing paleoenvironmental reconstructions through biotic changes and geochemical analysis.

2. Geological setting

The KD mountain range is an active fold belt between NE Iran and Turkmenistan. The Iranian part of the KD was formed after the early Cimmerian orogeny following the closure of the Paleotethys Ocean during the Late Triassic (Fig. 1a; Berberian and King, 1981; Stampfli, 2000; Stampfli and Kozur, 2007; Stampfli et al., 1991, 2001; Robert et al., 2014). In this area of the northern Tethys margin, Mesozoic and Paleogene lithostratigraphic units were deposited following the Mid-Jurassic opening of the south Caspian basin along the suture of the Paleotethys (Fig. 1b; e.g., Stöcklin, 1968; Berberian and King, 1981).

Central Iran consists of several tectonic blocks or microplates, which are collectively called the Central-East Iranian Microcontinent (CEIM; Aghanabati 2004). This area has revealed a complicated tectonic history since the Triassic (e.g., Bagheri and Stampfli, 2008). During the Late Cretaceous, these microplates were separated from the southern Eurasian margin, and small oceanic basins were formed around the CEIM (Fig. 1c; Robert et al., 2014).

During the Jurassic - Late Cretaceous, the YB was located south of the KD basin, and was not so far from the southern margin of the south Caspian basin. The KD basin was closed and inverted in the Cenozoic through the subsequent convergence between the Arabian and Eurasian plates due to the subduction of the Neotethyan Ocean. Thereafter, the YB was located farther from the KD basin because of the Late Mesozoic-Early Cenozoic anti-clockwise rotation of the Lut block (Fig. 1d; e.g., Stöcklin, 1968; Berberian and King, 1981; Stampfli and Borel, 2004; Bagheri, 2007). The YB now represents the western microplate of the CEIM (Fig. 2a; Takin, 1972; Aghanabati, 2004; Bagheri and Stampfli, 2008; Gheiasvand et al., 2020).

Five Lower Cretaceous stratigraphic sections of the KD basin and YB were investigated (Fig. 2a): Tirgan village, Amirabad and Padeha stratigraphic sections in the KD basin (Fig. 2b), as well as the Tamer and Tehr stratigraphic sections in the YB (Fig. 2c). Information on the geological setting of the stratigraphic sections regarding lithostratigraphy and paleontology, except for the Padeha section, has been published already (see Gheiasvand et al., 2018, 2019, 2020) and we give a short description of them in the following paragraph.

2.1. KD (Kopet-Dagh)

The measured sections of this area are located in the central to easternmost part of the KD mountain range (Khorasan-e-Razavi Province), including the Tirgan Fm and lower parts of the Sarcheshmeh Fm (Fig. 3).

The first investigated section is the Tirgan village section (37°07′11″N; 59°18′45″E) located 3 km south of the Tirgan village. This section is composed of bioclastic limestones of the Tirgan Fm. The limestone beds of this formation are subdivided into four units (Unit 1 to 4). The second stratigraphic section is the Amirabad section (36°33′40″N; 60°04′02″E) located about 20 km east of the Gojgi village. The Amirabad section is subdivided into three units. These units are named respectively from base to top of the section: platform carbonates, hemiplegic carbonates, and shales of the Sarcheshmeh Fm. Here, the Tirgan Fm is about 40 m and dominated by fossiliferous limestones, shale, and argillaceous and marly limestones. The most eastern studied succession is the Padeha section, 13 km southeast of the Mazdavand county (36°05′39″N; 60°39′19″E). In this section, 25 meters of the lower and upper parts of the Tirgan Fm, is mainly composed of brown-gray oolitic and fossiliferous limestones and marls (Fig. 4).

In these sections, the carbonate successions of the Tirgan Fm overlie clastic and evaporitic deposits of the Shourijeh Fm and are covered by shaly deposits of the Sarcheshmeh

Fm (Fig. 3). The thickness of the Tirgan Fm decreases towards the east of the KD mountain range (towards the Padeha section). For better correlations through the area, the sample spacing of the Sarcheshmeh Fm was increased from the central to the easternmost part of the KD range.

2.2. YB (Yazd Block)

The Lower Cretaceous marine successions in the YB are known under different informal names; e.g., the Shah Kuh formation (Khur area) or the Taft formation (Yazd area). For this study we have investigated two stratigraphic sections located in the Yazd province, west of Taft county (Fig. 2c), including the Taft fm. The first section is the Tamer section (Fig. 3), which is a composite section. The Tamer section has been sampled and studied for its lower part, 20 km west of Taft county (31°42′48″N; 54°06′57″E), and for its upper part, 7 km ESE of the lower part (31°41′38″N; 54°11′08″E). In general, rudist-rich limestones, marly limestones, and dolomitized limestones are dominant lithologies of the Taft formation. The second stratigraphic section is the Tehr section (31°37′17″N; 53°50′57″E) located 50 km west of Taft county. This section is dominated by thick-bedded bioclastic limestones, including rudists, calcareous algae, and foraminifera (Fig. 3).

The investigated stratigraphic sections include the carbonate successions of the Taft fm, which overlie the clastic deposits of the Sangestan fm and are covered by shaly deposits of the Darreh-Zanjir fm.

3. Material and methods

3.1. Microfacies

A total of approximately 640 carbonate rock samples were processed to obtain thin sections and investigation of them was performed by using conventional optical microscope at the laboratory of the University of Lausanne, the Ferdowsi University of Mashhad, and the Association Dolomieu in Grenoble. The distribution of microfacies associations were examined following the Arnaud-Vanneau and Arnaud (2005) classification (Table 1).

3.2. Paleontology and paleobiogeography

In addition to the published paleontology data through sections including benthic foraminifera and colomiellids (Gheiasvand et al., 2018, 2019, 2020), some microfossils were determined in the thin sections from the Amirabad and Padeha stratigraphic sections (in the KD). These microfossils include benthic foraminifera, planktonic organisms such as colomiellids, and calcareous algae. Some ammonites were also collected from the base of the Darreh-Zanjir formation of the Tamer stratigraphic section (in the YB).

The shallow-water carbonates containing eleven species of benthic foraminifera and hemipelagic sediments including colomiellids were examined for paleobiogeography. These cosmopolitan microfossils are recognised as biostratigraphic indices for the Early Cretaceous. Twenty-six references for the micropaleontology studies of benthic foraminifera were used (Poroshina, 1976; Kovatcheva, 1979; Arnaud-Vanneau and Silter, 1995; Reháková et al., 1996; Lesná, 1997; Neagu, 1997; Chartrousse and Masse, 1998; Loeblich and Tappan, 1988; Bodrogi, 1999; Neagu and Cîrnaru, 2002; Voznesenskii et al., 2002; Husinec and Sokac, 2006; Velić, 2007; Afghah and Fanati Rashidi, 2007; Bruni et al., 2007; Krajewski and Olszewska, 2007; Sudar et al., 2008; Tawadros, 2011; Hfaiedh et al., 2013; Dragastan et al., 2014; Hosseini, 2014; Schlagintweit et al., 2016; Yavarmanesh et al., 2017; Gheiasvand et al., 2018, 2019, 2020), and five references for the studies of colomiellids were compiled (Longoria, 1972; Longoria and Gamper, 1974; Trejo, 1975; Zghal et al., 1996; Gheiasvand et

al., 2019). This micropaleontological database reported on the Panalesis plate tectonic model (see Vérard, 2018), and represents 40 localities on the paleomaps at 140, 130 and 120 Ma. The data is shown in paleomagnetic (Mag) coordinates, which are transferred back in time using different tectonic elements.

3.3. Stable isotope analysis

For the carbon and oxygen stable isotope analysis, 255 bulk-rock samples were processed. We used samples including wackestone, mudstone, or the micritic matrix of mud-dominated packstone and floatstone. Samples showing petrographic evidence of diagenetic alteration, fractures, or cement-filled cavities and veins were avoided. The $\delta^{13}C$ and $\delta^{18}O$ values were obtained from microdrilled powder of the rock slices using the Spangenberg et al. (2014) procedure at the Institute of Earth Surface Dynamics of the University of Lausanne. Analyses of the samples were carried out using a Thermo Fisher Scientific Gas-Bench II preparation device interfaced with a Thermo Fisher Scientific Delta Plus XL continuous flow isotope ratio mass spectrometer (IRMS). The stable isotope ratios reported in the delta (δ) notation as the per-mil (‰) deviation relative to the Vienna Pee Dee Belemnite standard (VPDB). The analytical uncertainty (2σ) was assessed using the international calcite standard NBS-19 and the laboratory standard Carrara Marble as not larger than ±0.05 ‰ for $\delta^{13}C$ and ±0.1 ‰ for $\delta^{18}O$.

3.4. Phosphorus content

The P accumulation was characterised using 109 bulk-rock carbonate samples at the University of Lausanne. The samples were crushed to obtain a fine, homogeneous powder. Approximately 100 mg of every powder was mixed with 0.5 ml of MgNO3 and dried in an oven at 100 °C for 30 minutes, and then at 550 °C for 2 hours and 30 minutes. After cooling,

10 ml of HCl 1mol was added and placed under constant shaking for at least 16 hours. The solution was filtrated and analysed following the Eaton et al. (1995) ascorbic acid procedure. The final solution obtained was studied by a spectrophotometer (UV/Vis Perkin Elmer Lambda 25 spectrophotometer) to determine the phosphorous accumulation. The concentration of PO4 was obtained by calibration with known internal standard solutions and reported in mg/L, providing precision better than 5% (see also Bodin et al., 2006a).

4. Results

4.1. Stratigraphic trends in microfacies

In our studied sections, ten main microfacies types together with evidence of reworking (R) and dolomitisation (D; see Table 1 and Fig. 3) have been identified.

The microfacies are indicated along a rimmed platform model (Fig. 5; F1 to F8, F10 and F11). According to the interpreted paleobathymetry, these kinds of microfacies are grouped into three categories, MF1 to MF3, which reflect the environmental position of organisms and carbonate components. They are located on the shallow-water platform and outer shelf beyond the platform margin. MF1 (F1 to F4) represents outer-shelf, MF2 (F5 to F7) outer-platform (platform margin), and MF3 (F8 and F10) inner-platform (subtidal and intertidal, including lagoon and tidal flat). The deepest environment is defined by marl and marly limestone, including less than 50% of pelagic organisms (e.g., calpionellids, radiolarians, calcispherids, ammonites, sponge spicules; F1). The shallowest part of the platform shows supralittoral facies, which is specified by F11 (Figs. 3 and 5; see also Bonvallet, 2015; Bonvallet et al., 2019 and Gheiasvand et al., 2019).

4.1.1. KD (Kopet-Dagh)

The successions of the Tirgan Fm in the KD mountain range show 10 main microfacies types. The diversity of microfacies decreases towards the most eastern studied succession in the Padeha section (Fig. 3).

In the Amirabad section, 8 microfacies types (F1, F3 to F7, F10 and F11) with evidence of reworking (R) are recognised (Fig. 3). The vertical succession of the Amirabad section starts with bioclastic limestones, including reworked elements (lag), which quickly changes to an outer-platform position close to 8 m. From this level onwards, the succession is mainly composed of oolitic facies (F6), with packstone and grainstone. The dominant components of these deposits are oolites. In addition, we found coral debris, bryozoans and echinoderm fragments, and occasionally annelids. Near 18 m, a variation towards proximal type microfacies begins (F10 and F11a) and terminates with an emersion surface. This level of emersion is characterised by the presence of karstic microcaves at around 22 m. Then, the microfacies shift again to deeper types (F6; outer-platform). From 26 m onwards, an interval of deep-water facies is defined (F1), consisting of the outer-shelf facies and covers the top of the Tirgan Fm and the lower parts of the Sarcheshmeh Fm.

The Padeha section consists of a succession of 3 microfacies types (F1, F4 and F6), with evidence of reworking (R). The microfacies display an initial phase of marine deepening, which is identified by the outer-shelf facies, followed by a change to the outer-platform facies with intercalations of reworked facies between 15 and 22 m (Fig. 3). At the top of the Tirgan Fm, the microfacies shift again to deep-water types. Bryozoans and echinoderm fragments are dominant components of these deposits, which are overlain by an interval of the outer-shelf facies (F1) in the Sarcheshmeh Fm.

In this study, the types of microfacies of the published Tirgan village section (Gheiasvand et al., 2019) are compared with the other stratigraphic sections. In the Tirgan

village section 8 microfacies associations (F1 to F4, F6, F8, F10 and F11) were recognised, together with evidence of reworking (R) and dolomitisation (D).

4.1.2. YB (Yazd Block)

The successions of the Taft fm in the YB show 6 main microfacies types (Fig. 3).

Two microfacies (F5 and F8) with evidence of dolomitisation (D) are recognised in the Tamer section. The Tamer section (Fig. 3) presents an interval of dolomitized limestone at the base of the section. From 70 m onwards, a shift towards inner-platform facies is observed (F8), with grainstone intercalations (F5) and partly dolomitized facies (D). The deposits are mainly composed of miliolids, conical orbitolinids and rudists. The Taft fm underlies the Darreh-Zanjir Fm, which displays the outer-shelf facies in the lower part.

The Tehr section (Fig. 3) exhibits a succession of 6 microfacies types (F1, F3 to F6 and F8) and also evidence of reworking (R). The base of the Tehr section shows marine deepening to the outer-shelf facies (F3), followed by outer-platform grainstone (F5) with one packstone/grainstone intercalation. From 25 to 100 m, the microfacies associations change again to deeper types (F3; outer-shelf), with intercalations of reworked and outer-platform facies. Near 110 m and onwards, the deposits are mainly composed of outer-platform grainstone, with intercalations of lagoonal and outer-shelf facies. The microfacies shift again to deep-water types between 175 and 250 m, and an alternation between outer-inner-platform and outer-shelf microfacies is observed between 250 and 465 m. Dominant components of these deposits are miliolids, conical orbitolinids, oolites, and rudists, with some annelids, calcareous sponges, bryozoans and echinoderm fragments. From 480 m to the top of the section, lagoonal facies are mainly recognised.

4.2. Stratigraphic trends in carbon and oxygen isotope record

The results of the carbonate stable isotopes for the studied sections are shown on Figs. 6 and 7. Based on our results, the deposits of the Tirgan, Taft and Sarcheshmeh formations record the worldwide major environmental changes that affected many Lower Cretaceous carbonate platforms during the oceanic anoxic events and associated with the $\delta^{13}C$ perturbations, like the latest early to the late Valanginian Weissert, the latest Hauterivian Faraoni, the early Aptian OAE1a (or Selli event) and the late Aptian Fallot events. Likely the late Aptian to early Albian OAE1b (Jacob and Paquier events) and latest early to the late Aptian Noir events are also registered in these successions.

4.2.1. KD (Kopet-Dagh)

In the Amirabad section, the stable isotope record relates to the samples of the Tirgan Fm and lower parts of the Sarcheshmeh Fm (Fig. 6a). The $\delta^{13}C$ values are characterised by a decrease at the base of the Tirgan Fm, followed by a small increase at around 5 m. They rapidly decrease again and reach minimum values at 20 m (karstification surface). Above this level, the values rise again and are followed by two maximum and minimum peaks at about 35 m (likely the late Aptian to early Albian OAE1b event). The rest of the $\delta^{13}C$ record towards the top of the Tirgan Fm shows a decrease, followed by a slow increase. The values in the Sarcheshmeh Fm are characterised by a gradual and irregular increase of values between around 40 and 80 m before reaching a maximum value of 4‰ at 80 m. The $\delta^{18}O$ record shows an irregular evolution, ranging between about -6 and -3‰ for the Tirgan Fm, and around -8 and -5‰ for the studied parts of the Sarcheshmeh Fm.

Stable isotopes of the Padeha section are mostly related to the Tirgan Fm and lower parts of the Sarcheshmeh Fm (Fig. 6a). This section shows the $\delta^{13}C$ record with a decrease from the base of the Tirgan Fm, followed by an increase at around 15 m towards the top of the formation. They decrease again and reach minimum values at 30 m, an interval of the

Sarcheshmeh Fm. From 30 m onwards, the $\delta^{13}C$ values increase and decrease again to reach a minimum at 37 m (interpreted as the early Aptian OAE1a event; interval between 30 and 37 m). They gradually increase and reach maximum values at around 55 m (likely latest early to the late Aptian Noir event), rapidly followed by a decrease again and reach minimum values at about 75 m (the late Aptian Fallot event). Above this level, the record towards the top of the section is defined by an increase, followed by a slow decrease. Like the previous section, the $\delta^{18}O$ record shows an irregular pattern of values. They range between ca. -8 and 0‰ for the Tirgan Fm, and ca. -9 and -5‰ for the lower parts of the Sarcheshmeh Fm.

The stable isotope results from the published Tirgan village section (Gheiasvand et al., 2019) are compared with the other stratigraphic sections from the KD mountain range (Fig. 6a). This section shows the $\delta^{13}C$ record with the positive excursions between around 115 and 240 m (the latest early to the late Valanginian Weissert event). The values increase again towards 390 m (the latest Hauterivian Faraoni). Above 440 m, a decrease occurs which is followed by the irregular evolution in the $\delta^{13}C$ record up to a decrease at 565 m. We also recognised the late Aptian Fallot event at 565 m of the Tirgan village section, well correlated with the Fallot event of the Padeha section. The trend for the early Aptian is less well reproduced in the Tirgan village section and this may be related to the short hiatus that exists in the successions. The $\delta^{18}O$ record of the Tirgan village section shows an irregular evolution, ranging between about -5 and 0‰ for 450 m; these values are followed by a more regular pattern between -6 and -3‰ for the remainder of the section.

4.2.2. YB (Yazd Block)

The Tamer section is characterised by the initial $\delta^{13}C$ record increasing gradually from 20 m to 120 m (Fig. 7a). This is followed by a decrease and reaches minimum values at around 160 m. Above this level, the Taft fm shows a positive excursion of approximately 2‰

starting. The $\delta^{13}C$ values start to decrease at around 190 m and reach minimum values at around 250 m (correlated with the early Aptian OAE1a event). They increase again between ca. 250 and 350 m. From 350 m onwards, they decrease and then start to increase at the base of the Darreh-Zanjir fm. An irregular trend of values is related to the $\delta^{18}O$ record which is defined between about -18 and -4‰ for the first part of the section (up to 180 m). This interval goes on with a nearly steady trend of values between -8 and -3‰ for the rest of the section.

In the YB, the samples of the Tehr section are excluded for the stable isotope analysis, because they mostly consist of grainstone with cement-filled cavities.

4.3. Stratigraphic trends in phosphorus content

4.3.1. KD (Kopet-Dagh)

The base of the Tirgan Fm is characterised by a positive peak of the P values in the Amirabad stratigraphic section (Fig. 6a). This is followed by smaller values, reaching a minimum of 177 ppm. A second increase reaches maximum values around 565 ppm. The upper part of the Tirgan Fm shows a progressive decrease down to a minimum content at around 35 m, followed by a positive peak towards the top of the Tirgan Fm. The P content attains variable values in the Sarcheshmeh Fm, with a maximum of 400 ppm and a minimum of 100 ppm.

The Padeha section shows a P record with a positive peak of approximately 480 ppm at around 15 m (Fig. 6a). The P values continue with a sharp decrease, reaching a minimum of 157 ppm towards the top of the Tirgan Fm. This phase is followed by an increase at the uppermost part of the Tirgan Fm and at the base of the Sarcheshmeh Fm. The P content in the Sarcheshmeh Fm is variable between around 160 and 490 ppm.

4.3.2. YB (Yazd Block)

The Tamer section starts with a decrease of the P content and reaches minimum values around 17 ppm at 20 m of the section (Fig. 7a). This interval is followed by an increase to reach a maximum of 64 ppm around 80 m. A second decrease is observed and attains minimum values around 14 ppm. Above this phase, the P content remains low and steady between 9 and 26 ppm in the Taft fm and reaches higher values with a maximum of 64 ppm at around 250 m. In the interval above 250 m, they nearly rapidly decrease again, reaching a minimum of 9 ppm at 290 m. The steadier values of P accumulation are observed between 9 and 17 ppm, followed by an increase at the top of the Taft fm.

The base of the Taft fm in the Tehr section is characterised by a positive peak in P values, followed by a decrease reaching a minimum of 29 ppm at around 45 m (Fig. 7a). The P values start to sharply increase from 45 m and attain maximum values of 370 ppm at around 52 m. A decreasing trend is observed in the interval between 45 and 215 m, followed by a positive peak, attaining a maximum of 137 ppm. This phase is followed again by a decrease, and reaches minimum values of 25 ppm at 330 m. Above this level, an increase in P values is recorded, followed by a steady and irregular evolution up to top of the section.

4.4. Biostratigraphy, reconstruction models of the evolution of the deposits containing index microfossils and paleobiogeographic provinces

Biostratigraphy is here mostly based on benthic foraminiferal species and planktonic microfossils (see Table 2).

In this work, some new microfossils including planktonic organisms, such as colomiellids, radiolarians, and calcispherids were identified from the upper part of the Tirgan Fm in the Amirabad section (Table 2). According to these microfossils, a planktonic assemblage zone is

defined as found in the Tirgan village section (Fig. 6a). Based on *Cadosina* sp. (at 24 m), *Colomiella* sp. (at 24 m, 33 m, 37 m and 40 m), *C. mexicana* (at 33 m and 37 m) and *Hedbergella* sp. (at 40 m), the recognition of the late Aptian to Albian for this thickness is possible (24 to 40 m; Longoria 1972, 1973; Longoria and Gamper 1974; Trejo, 1975; Fekete et al., 2017 and Gheiasvand et al, 2019). We also defined a stratigraphic range for the Padeha section, where the first appearance of orbitolinidae occurs at 15 m, which coincides with the presence of *Kopetdagaria sphaerica*. This algae species is also observed at about 19.4 m and 25 m and, among orbitolinidae, « *Dictyoconus » pachymarginalis* is recognised at 19.4 m. These microfossils of the Padeha section suggest a late Barremian? to early Aptian age for the Tirgan Fm (e.g., Schroeder, 1965; see also Table 2). The first appearance of orbitolinidae has been also observed in the other sections of the KD basin and indicates a Barremian - Aptian age. The appearance of orbitolinidae is a particularly good marker in the Tirgan village section where the shallow-water carbonate succession extends also below the Barremian age. Unfortunately, it was not possible to identify the species of orbitolinidae from the Sarcheshmeh Fm in the Padeha section because the embryonic apparatus was not visible. However, according to the stratigraphic position, the lower parts of the Sarcheshmeh Fm can be referred to the lower Aptian. Furthermore, several ammonites at the base of the Darreh-Zanjir fm from the Tamer section, suggest a middle to late Albian age, based on the presence of *Anisoceras* sp., *Beudanticeras* sp., *Beudanticeras* cf. *laevigatum*, *Beudanticeras* cf. *beudanti*, *Eotetragonites* sp.?, *Epihoplites* (*Metaclavites*) *compressus*, *Idiohamites* sp., Phylloceratidae, *Tetragonites* sp. (Seyed-Emami and Immel, 1995; Matrion, 2010). This data indicates a stratigraphic hiatus at the top of the Taft fm, comprising the late Aptian to early Albian.

For the reconstructed distribution models of the microfossils, several benthic foraminifera of the shallow-water carbonates and colomiellids of the hemipelagic sediments

were considered. Some of them have never been recorded in the northern Neotethys (e.g., *Orbitolinopsis nikolovi*, *Feurtillia gracilis* and *Colomiella* sp.; see also Tables 3, 4 and 5, and Gheiasvand et al., 2018, 2019, 2020). The ages of microfossils are completed using stratigraphic information from the literature and are simplified for the sake of paleobiogeographic reconstructions. For this study, we considered the coeval occurrences of microfossils, including Valanginian (*Decussoloculina barbui*), late Valanginian (*Feurtillia gracilis*), Hauterivian (*Bolivinopsis labeosa*, *Campanellula capuensis*), early Aptian (*Conorbinella azerbaidjanica*, *Orbitolinopsis nikolovi*, *Arenobulimina cochleata*), and late Aptian associations (*Arenobulimina meltae*, *Colomiella* sp., *Martinotiella jucunda*, *Mayncina bulgarica* and *Simplorbitolina manasi*). This data outlines new global paleobiogeographic reconstruction models for the different areas, including benthic foraminifera and colomiellids for the Valanginian, Hauterivian and Aptian. Some of the paleogeographic clusters that specify the paleobiogeographic provinces are described (Tables 3, 4 and 5 and Figs. 8a- c).

The known palaeobiogeographic provinces of the benthic foraminifera and colomiellids indicate that they belong to cosmopolitan forms. Occurrences of them at 120, 130 and 140 Ma are marked by distinctive paleogeographic clusters of marine biota. According to paleoceanographic settings of these paleogeographic clusters, we defined six faunal provinces (northern and southern Neotethys, northern and southern Alpine Tethys, Gulf of Mexico and northern Pacific Ocean). The Valanginian fauna are rare in the KD basin and YB (northern Neotethys) and some of them, such as *Decussoloculina barbui* were observed in the adjacent paleobiogeographic province (e.g., in the southern Alpine Tethys; see Fig. 8a). The comparison of different areas shows diversified ecosystems for the late Valanginian to the Aptian (Figs. 8b, c). It is remarkable that the relative abundance of index foraminifera decreases in the southern hemisphere and colomiellidae are absent in this area.

5. Discussions and interpretations

5.1. Age models of the Lower Cretaceous successions using biostratigraphic results and changes of the $\delta^{13}C$

Here, the ages of the studied Lower Cretaceous successions are identified by index microfossils (benthic foraminifera and colomiellids) and then refined using changes of the $\delta^{13}C$. A three-point moving average of the $\delta^{13}C$ from the central to the easternmost part of the KD mountain range and the $\delta^{13}C$ records in the YB are correlated with the bulk-rock $\delta^{13}C$ values recorded in a reference section from southeastern France along the northern Alpine Tethys margin (Fig. 9; Föllmi, et al., 2006). These correlations helped to identify excursions and strengthen the calibration of the biostratigraphic results. They are particularly good for the positive excursion of the late Valanginian where the Weissert event is recognised. During the Hauterivian, the general trend of the values is more negative, reaching a positive shift in the $\delta^{13}C$ values at the top of this time interval. Appropriate similarity of values also exists for the Barremian and Aptian,. Furthermore, the correlations of the obtained $\delta^{13}C$ values from the sections and the reference record allow us to refine the ages of the Tirgan and Taft formations based on the benthic foraminifera and planktonic organisms. As shown on Fig. 6a and 7a, microfossils are grouped around the *Feurtillia gracilis* range zone (late Valanginian), the *Campanellula capuensis* range zone (late Hauterivian– Barremian), the Orbitolinid assemblage zone (early Aptian to late Aptian) and the Planktonic assemblage zone (late Aptian to Albian) in the KD basin, as well as the assemblages 1 (Valanginian? – Hauterivian/ or late Barremian to early Aptian) and assemblages 2 (late Barremian– late Aptian/ or late Aptian) in the YB. Time intervals of the biozones are refined by changes of the $\delta^{13}C$ trend and their correlation. For example, in the Tirgan village section, the first and last appearance of *Feurtillia gracilis* are between around 140 and 230 m, which this interval of the late

Valanginian is refined by the positive excursion at around 120 to 240 m. According to our results, several age limits through the stratigraphic sections were distinguished. However, it was notable that fossil indices of some intervals were not recognised and the events through any section were also partly constrained, which may be related to the presence of one or more hiatuses for these successions (see Figs. 6a, b and 7a, b and also Gheiasvand et al., 2019, 2020). On the other hand, there is a diachrony in ages at the base and the top of the Tirgan and Taft formations and the sections are not easily correlatable (Figs. 6b and 7b). For a better view of these results, the stratigraphy of the studied Lower Cretaceous successions in the KD basin and Central Iran (YB) main zones, and also their equivalent lithostratigraphic units in other main parts of Iran, Zagros (southern Neotethys) and Alborz (northern Neotethys), are shown on Fig. 10 (see Immel et al., 1997; Aghanabati and Rezaee, 2009). This figure shows that the Tirgan and Taft formations boundaries are not isochronous but diachronous. The evaluation of our fauna also clearly demonstrated this reality. According to Immel et al. (1997), the base of the Tirgan Fm starts at the earliest Cretaceous (Hauterivian?) in the west of the KD basin and at the upper Barremian in the east, whereas the top of this formation ends at the upper Barremian in the western part and at the lower Aptian in the eastern part. In this research, we can therefore improve the ages of the formational boundaries as shown on Fig. 10. According to our studies, the base of the Tirgan Fm can start at the Berriasian? to lower Valanginian and end in the upper Aptian to Albian from the central towards the eastern part of the KD basin. Here, the top of the Tirgan Fm corresponds to an erosional surface that removes parts of the Sarcheshmeh series. Normally, the Sarcheshmeh Fm consists of two informal members; the lower marly and the upper shaly member. This formation starts with shaly member through our sections that may explain why in our studies the Sarcheshmeh Fm starts with the younger series. The ages of the formational boundaries and the extent of the hiatuses of the Taft formation in the YB are also modified according to our data (Fig. 10).

5.2. The Early Cretaceous diachronous transgressive event in the KD basin and YB

Using the proposed age models, the studied stratigraphic sections suggest different settings of the Lower Cretaceous successions in NE and Central Iran affected by a diachronous transgressive event in an active extensional tectonic regime, likely following the Cimmerian phase of epi-orogenesis in Iran during the Jurassic (e.g., Wilmsen et al., 2009, 2015). These movements were related to the opening/subsidence of the Caspian oceanic basin (e.g., Brunet et al., 2003; Wilmsen et al., 2018). This opening extended eastward to the Farah basin in Afghanistan (Siehl, 2017 and Vérard, 2018; Fig. 11), whereas tectonic events took place in Central Afghanistan. In this area, a major orogenic period started in the Late Jurassic, and ended with the deposition of the Lower Cretaceous red clastic successions (continental molasses) characteristic of Central Afghanistan (Brunet et al., 2015). Rifting also started in the Early Cretaceous around the future central Iranian microcontinent, leading to the opening of small oceanic basins in the Late Cretaceous (Bagheri and Stampfli, 2008).

We tracked the base level facies of the Tirgan and Taft formations to define the onlap surfaces in the KD mountain range and YB. Marine limestones, shales and marls at the base of these formations show a change of the continental area due to a marine transgression, which is shown on Figs. 12 and 13. The basal marine beds of the Tirgan and Taft formations onlap the clastic and evaporite deposits of the underlying Shourijeh Fm and Sangestan fm respectively in the KD range and YB area. Following the basal sequence boundary (Sb1), the progressive onlaps of outer-shelf or inner to outer- platform successions mark a relative rise in sea level (e.g., Kendall and Lerche, 1988) with a consequent diachronous basal age of the Tirgan and Taft formations. The variability of observed facies and thickness inside the formations along different sections (eg., Tirgan fm) can be related to a variations in subsidence rate and to the inherited paleorelief physiography. Field observations show that the

thickness of the Tirgan Fm drastically reduces from the Tirgan village section (640 m) towards the Padeha section (25 m), and finally the Tirgan Fm disappears in the eastern part of the KD mountain range (Fig. 12a; see also Gheiasvand et al., 2019). On the other hand, Google Earth images in the area of the Tirgan Fm type section shows a pronounced westward onlap of the Tirgan deposits onto the Shurijeh Fm (Fig. 12b). This means that the base of the Tirgan Fm becomes younger towards the western part of the KD basin and explains why the Tirgan village section starts with older deposits (Berriasian? to lower Valanginian) than the Tirgan Fm type section (upper Barremian? to lower Aptian). The base of the Tirgan village section also shows an older age than the base of the Amirabad and Padeha sections, due to a mixture of subsidence effects and paleoreliefs in the KD basin (Fig. 12c), with the base of the Tirgan Fm becoming younger towards the eastern part of the basin.

Also in the YB, the Taft fm in the Tehr section shows a pronounced southward onlap pattern onto the deposits of the Sangestan fm (Fig. 13a). The base of the Taft fm therefore becomes younger to the south, and this explains why the Tamer section starts with older deposits than the Tehr section (Fig. 13b).

In the whole area, the upper boundary of the Tirgan and Taft formations is an emersion surfaces with evidence of erosion and karstification features, including microcaves. Finally, these sequence boundaries are covered by shaly deposits of the Sarcheshmeh and Darreh-Zanjir formations.

5.3. Microfacies and carbon and oxygen isotope evolution

The distribution of the microfacies associations and their evolution in time provide information on the morphology of the studied platforms and their evolution. The changes of microfacies and environmental markers show that the evolution of the KD and YB platforms is similar to those in the other Tethyan Platforms (e.g., Subalpine and Helvetic platforms; see

Bonvallet, 2015). Here, phases of shallow-water carbonate development are present in the late Valanginian to early Hauterivian, the early to middle late Barremian, and the late early to the late Aptian, interspersed with deep-water, open-marine phases.

The Tirgan and Taft formations are followed by a transgressive phase, which can be accompanied by the sedimentation of hemipelagic and deep-water facies above the emersion surfaces. During the Valanginian to the Albian, the successions of the Tirgan and Taft formations show the morphology of a rimmed platform by the presence of lagoonal facies rimmed by oolitic shoals and scattered patch-reefs. These patch-reefs are composed by corals, rudists, algae, bryozoans, and sponges (Bonvallet et al., 2019). These deposits reflect the environmental location of ecosystems from the outer-shelf to inner-shelf. The successions of the Tirgan Fm in the KD mountain range show 10 main microfacies types and the Taft fm in the YB show 6 types, in which the environmental diversity is less than in the successions in the KD. In the Amirabad section, the contact between the hemipelagic sediments of the Tirgan Fm and the shallow-water carbonates of this formation represents an emersion surface, which is specified by karstification features, including microcaves, covered by paleosols (Fig. 14; see also Gheiasvand et al., 2018).

The carbon isotope variations from the Lower Cretaceous successions show that oceanic anoxic events are frequent and followed by the variations of the carbon cycle and pCO_2, which triggered climatic perturbations during this time (Schlanger and Jenkyns, 1976; Jenkyns, 2010; Bonvallet, 2015). They also show some positive $\delta^{13}C$ excursions and many minor events in the Lower Cretaceous successions of the KD basin and YB. The distribution and evolution of facies and microfacies are associated with sea-level, geochemistry and paleotopographic changes and with paleoceanographic conditions. The presence of positive and negative carbon stable isotope excursions is compatible with some microfacies associations. The positive shifts of the $\delta^{13}C$ recorded in the Tirgan village section and Tamer

section coincides with the onset of the lagoonal facies (MF3; Fig. 15), which may be related to an increase in aragonitic components (e.g., Föllmi et al., 2006, 2007). In fact, the abundance of green algae, rudists and other mollusk groups such as gastropods are originally sources for the aragonitic components (e.g., Bandel, 1990; Steuber, 2002; Scholle and Ulmer-Scholle, 2003; Flügel, 2004; Skelton and Gili, 2012; see also Bonvallet et al., 2019). A good correspondence is observed between reconstructed aragonite content and the $\delta^{13}C$ records through our sections (see Figs. 3, 6a and 7a). The most negative values coincide with oolitic facies (MF2; Fig. 15) which are grainstones and show early cementation (e.g. meteoric cement). The $\delta^{13}C$ records and trends towards negative values also occur in relation to the presence of emersion surfaces (see Bonvallet, 2015). The phase of erosion at 22 m of the Amirabad section is well reflected in the carbon isotope record (Fig. 6a). Dolomitization is also revealed in the oxygen isotope record. This process is widespread in the interval between 400 and 500 m of the Tirgan village section and the base (10 to 40 m) of the Tamer section. In these intervals, the negative $\delta^{18}O$ values, the presence of saddle dolomite cement, non-planar texture and, coarse crystal size are evidence of a late diagenetic dolomitization phase at higher temperatures conditions (Machel 2004; Davies and Smith 2006; Gheiasvand et al., 2019).

5.4. Phosphorus content and photozoan to heterozoan assemblages

The allochem content and the P accumulation of the carbonate successions are used here to indicate trophic levels. Based on our studies, these areas experience changes from photozoan to heterozoan assemblages several times during the Early Cretaceous (see Figs. 16a- d). The general decrease in P content is correlated with light-dependent fauna such as green algae and corals, and represents a typical oligotrophic, photozoan association. Rudist-rich photozoan limestones are also correlated with a decrease in P content as well expressed through the rudist-rich- Tamer and Tehr sections located in the YB (see Fig. 7a). Although the

rudist dependence on trophic levels is problematic here, the 'Rudist-rich photozoan limestones' are recorded in other studies (e.g., James, 1997; Föllmi et al., 2007; Bonvallet, 2015). Since most rudists are considered as heterotrophic suspension feeders, it is important to review the paleoecologic and paleoceanographic conditions of these organisms during different time intervals, and study deposits including them that despite of their being as heterozoan association can be parts of a photozoan carbonate platform with fauna such as green algae (see also Skelton and Gili, 2012; Michel et al., 2018). An increase in P content shows the dominant groups of light-independent fauna, such as bryozoans, sponges, echinoderms and annelids in the carbonate-producing ecosystem, and indicates a typical nutrient-rich phase (mesotrophic to eutrophic) of heterozoan association. *Lithocodium* is shown as forming part of the tropical platform biota which is recognised in the Tamer section. This organism is temporarily replaced by rudist-coral assemblages (Rameil et al., 2010), and represents an oligotrophic, photozoan association (Fig. 16c).

A shift from a photozoan to heterozoan association follows the effect of relative sea-level rise and high nutrient levels. In some areas the development of phosphate-rich sediments may also be a sign of eutrophication on the platform in relation to the drowning episode, such as the upper Hauterivian-lower Barremian deposits in the northern Tethyan margin (Helvetic realm; Bonvallet, 2015; Bodin et al., 2006b).

In the KD basin, the Lower Cretaceous platform shows a typically heterozoan assemblage during the late Barremian, followed by eutrophication during the transgressive phase. Phases of important heterozoan carbonate production are also recognised in the early Aptian, late early Aptian and late Aptian, which recorded in other localities of the Tethyan realm and interpreted as the consequence of global paleoceanographic changes (e.g., Helvetic platforms; Föllmi et al., 2006, 2007). In the Amirabad section, the Aptian exposure surface is locally covered by the deposition of phosphatic beds of the Tirgan Fm as

documented by a trend towards higher values. An important regressive phase near this surface led to the emersion of the carbonate platform, followed by the deposition of widespread hemipelagic sediments during the transgressive phase. The faunal associations indicate an increase in nutrient levels linked to the transgression (Figs. 14 and 16a). P content in the Tirgan Fm is generally higher than those in the Taft fm, which suggests the trophic levels were higher during the deposition of the Tirgan Fm successions.

The oligotrophic fauna as observed in the Tamer and Tehr sections (YB) is likely due to a change in climatic conditions towards dryer conditions. Photozoan organisms can produce carbonate and adapt well to lesser trophic levels which are also shown by the trends towards lesser values relative to the YB sections (Figs. 7a and 16c, d).

5.5. Described paleobiogegraphic provinces

In order to construct the paleomaps and discuss the paleogeographical distribution of the Early Cretaceous benthic foraminifera and colomiellids, data from other publications was extensively used (Tables 3, 4 and 5). Here, six faunal provinces are described. The hemipelagic sediments containing colomiellids belong to our four described provinces; northern and southern Neotethys, northern Pacific Ocean and Gulf of Mexico during the late Aptian to the Albian. In addition, the shallow-water carbonates containing benthic foraminifera belong to the five provinces, including northern and southern Neotethys, northern and southern Alpine Tethys, and northern Pacific Ocean during the Valanginian to the Albian. The microfossils distributions are related to the paleoceanographical situations, offering a new vision on the installation of the Lower Cretaceous carbonate successions in NE and Central Iran.

During the Early Cretaceous, the successions of the KD basin and YB are located approximately at the subtropical paleolatitudes, approximately at 30°N in the northern

Neotethyan region. At this time, a shallow marine carbonate platform is also developed in the northern and southern Alpine Tethys, whose assemblages are very similar to our areas; for example, the upper Berriasian-Aptian shelf carbonate platform in Romania, part of the Moesian Platform (Neagu, 1997; Neagu and Cîrnaru, 2002; Dragastan et al., 2014), the Berriasian - Valanginian platform in the Crimea Mountains (Krajewski and Olszewska, 2007), the Hauterivian-Barremian shallow-marine successions of the Adriatic platform, Croatia, southern Spain, Slovenia, Slovakia and Mljet Island in Croatia (Arnaud-Vanneau and Silter, 1995; Lesná, 1997; Husinec and Sokac, 2006; Velić, 2007), and the Barremian and Aptian Urgonian Limestones (e.g., Neagu, 1997; Sudar et al., 2008; Schlagintweit et al., 2016, see also Table 5). However, the regional formation of the carbonate platforms containing our index microfossils can be limited by local factors, such as changes in basin morphology, nutrient levels, water column stratification and hydrology.

The depositional environment related to the development of the platform during the Valanginian shows a dramatic reduction in carbonate production (e.g., Tennant et al., 2016), and an abundance and diversity of foraminiferal associations. All of them may be indicators of the carbonate platform demise in the mid-Valanginian through the western Tethys, which coincided with the perturbation of the global carbon cycle, and may have resulted in a regional or local extinction event, linked to the regional sea-level fall/uplifts (e.g., Erba et al., 2004; Erba, 2006; see also Ivanova et al., 2015).

The upper Valanginian and Hauterivian carbonate platforms and shallow marine carbonate platforms of the Barremian to Aptian, outcrop in many places around the world, from Europe to Iran, and from Africa to the Middle East, but also in the Pacific Ocean, South America, and Central and North America (e.g., Hashimoto and Matsumaru, 1971; Peybèrnes, 1979; Pudsey et al., 1985; Canérot et al, 1986; Arnaud et al., 1994, 1995, 2000; Arnaud-Vanneau et al., 1995; Vilas et al., 1995; Omana-Pulido and Pantoja-Alor, 1998; Bosellini et

al., 1999; Van Buchem et al., 2002; Barragan-Manzo and Diaz-Otero, 2004; Matsumaru, 2005; Sudar et al., 2008; Masse et al., 2009b; Amodio et al., 2013; Wilmsen et al., 2013; Morsilli et al, 2017; see also Bonvallet et al., 2019).

The benthic foraminifera that can be closely matched to the literature (*Arenobulimina meltae*, *A. cochleata*, *Bolivinopsis labeosa*, *Campanellula capuensis*, *Conorbinella azerbaidjanica*, *Decussoloculina barbui*, *Feurtillia gracilis*, *Mayncina bulgarica*, *M. jucunda, Orbitolinopsis nikolovi*, *Simplorbitolina manasi*), suggests that circulation may have been restricted during the Berriasian-Aptian with limited connections with the open oceans. The presence of colomiellids and *Campanellula capuensis* is highly significant and a clear marine connection with faunal migration routes between the Pacific oceanic realm and the eastern and western Tethys is certainly established in late Valanginian and Hauterivian times (e.g., Riccardi, 1991). The distribution patterns of microfossils show that systems of surface currents begin to develop during the late Valanginian (see Fig. 8), and their lateral migrations across the Pacific and Tethyan realms can be assumed. The mixed benthic foraminiferal faunas for the Early Cretaceous were previously recorded by Arnaud-Vanneau and Premoli Silva (1995), and Arnaud-Vanneau and Sliter (1995). These authors presented several taxa occurring between the margins of the Tethys and the Pacific oceanic realms for the Hauterivian to the Aptian. On the other hand, there was no apparent barrier for the migration of benthic faunas through the tropical oceans (see also Mancinelli and Chiocchini, 2006). Our models show that the Pacific oceanic realms received migrating faunas (benthic foraminifera and colomiellids) from the Tethys during the Hauterivian and Aptian, and the Gulf of Mexico received colomiellidae family during the late Aptian. The degree of microfossil mixing from the northern and southern Tethyan margins with the faunas from the Pacific Ocean and Gulf of Mexico is important for paleobiogeographic considerations. Similar mixing is recognised in the province from the southern Tethyan margin located in Italy, Tunisia, Algeria, Oman

and Iran that were paleogeographically close to the northern Tethyan margin during the Early Cretaceous.

6. Conclusions

The evolution of the Lower Cretaceous successions of the KD basin and YB (NE and Central Iran, along the northern Tethyan margin) were investigated with emphasis on the Tirgan and Taft formations. The Early Cretaceous biozone ages were refined using changes of the $\delta^{13}C$. In addition, the distribution of some microfacies associations, stable isotope perturbations and phosphorus (P) content were evaluated.

The Tirgan and Taft formations start with a transgressive phase, represented by a pronounced onlap pattern onto the Shurijeh and Sangestan formations. These successions reflect the different depositional environment from the outer-shelf to the inner-shelf, and display diachrony in ages at the base and the top of the stratigraphic successions, which suggests an effect of a long-term subsidence of the areas during the Early Cretaceous and/or the presence of paleoreliefs in the areas. The environmental diversity of the YB studied deposits is less than the ones in the KD. On the other hand, the study of the microfacies and environmental markers show the evolution on the KD and YB platforms is similar to those found in the other Tethyan carbonate platforms.

The Lower Cretaceous units of the KD basin and YB show some major positive $\delta^{13}C$ excursions and many minor events. The main Early Cretaceous events through our sections are rather well constrained and correlated with a reference record from southeastern France, along the northern Alpine Tethys, although the presence of hiatuses hamper in some cases a true correlation. The correlation with the Tethyan realm allows us to refine ages of our biostratigraphic zonal schemes and identify the equivalents of the following main events: the latest early to the late Valanginian Weissert, latest Hauterivian Faraoni, early Aptian OAE1a

and late Aptian Fallot. The late Aptian to early Albian OAE1b (Jacob and Paquier) and latest early to the late Aptian Noir events are also likely registered in these successions. Moreover, the allochem content of the successions and the P accumulation show that these areas experienced changes from photozoan to heterozoan assemblages several times during the Early Cretaceous, especially in NE Iran where a fast shift between oligotrophic and meso-eutrophic condition occurred. Phases of important heterozoan carbonate production are recognised in the early Aptian, late early Aptian and late Aptian, which are recorded in other localities of the Tethyan realm as the consequence of global paleoceanographic changes.

The defined palaeobiogeographic provinces of benthic foraminifera and colomiellids indicate that they belong to cosmopolitan forms. The comparison of different areas testifies of more diversified ecosystems from the late Valanginian towards the Aptian. The development of the platform during the Valanginian shows a dramatic reduction in carbonate production and a decrease in diversity and abundance of foraminiferal associations. The degree of mixing of microfossils from the northern and southern margins of the Tethys with the faunas from the Pacific Ocean and Gulf of Mexico has important repercussions on the paleobiogeography of that time. The new proposed models can provide an analogue for the evolution of depositional environments of the other Tethyan carbonate platforms.

Acknowledgments

In this study, we used samples collected for a research program at the Ferdowsi University of Mashhad. We thank this University for providing field equipment and some of the thin sections from carbonate samples (No., 3/39088). The first author acknowledges Ali Reza Ashouri for accepting her project so that the lithology and paleontology of the sections were studied and published during her mission at the Ferdowsi University. We appreciate the financial support of the University of Lausanne and Association Dolomieu for processing and

studying the samples. We sincerely regret that Karl Föllmi passed away before to see the final version of this manuscript, his input in the elaboration of this study was determinant. Here, we would like to show our great appreciation of his long and successful career at the service of the geosciences. We also gratefully acknowledge Annie Arnaud-Vanneau for providing information on samples and ages. We highly appreciate all the contributions of Thierry Adatte and Jorge Spangenberg for the carbon and oxygen stable isotope analysis, Tiffany Monnier for the phosphorus analysis and Antoine Pictet for the determination of the ammonites. We highly acknowledge the constructive reviews of two anonymous reviewers and the Editor, Ibrahim Uysal, who helped us to significantly improve the manuscript.

References

Afghah, M., Fanati Rashidi, R., 2007. Study of microfacies of the Kazhdomi Formation in northeast of Shiraz (Ab Chego mountain). Applied Geology 1, 17-22. (In Persian).

Afshar-Harb, A., 1979. The stratigraphy, Tectonics and Petroleum Geology of the Kopet Dagh Region, Northern Iran: Doctoral Imperial College of Science and Technology, University of London, London, England. 316 p.

Aghanabati, A., 2004. Geology of Iran. Tehran: Geological and Mine exploration Survey of Iran. 583 p. (In Persian).

Aghanabati, A., Rezaee, A., 2009. Correlation of lithostratigraphic units of Iran in major structural and sedimentology basins. National geoscience database of Iran.

Amodio, S., Ferreri, V., D'Argenio, B., 2013. Cyclostratigraphic and chronostratigraphic correlations in the Barremian–Aptian shallow-marine carbonates of the centralsouthern Apennines (Italy). Cretaceous Research 44, 132-156.

Arnaud, H., Arnaud-Vanneau, A., Bulot, L.G., Beck, C., MacSotay, O., Stephan, J.F., Vivas, V., 2000. Le Crétacé inférieur du Venezuela oriental: stratigraphie séquentielle des carbonates

sur la transversale Casanay-Maturin (Etats de Anzoátegui, Monagas et Sucre). Géol. Alpine 76, 3-81.

Arnaud, H., Bulot, L., Arnaud-Vanneau, A., 1994. Stratigraphie Séquentielle de l'Aptien et de l'Albien sur la Transversal Pico Garcia- Casanay (Venezuela oriental). Rapport Aguasuelos Ingenieria, Caracas, Venezuela. 77 p.

Arnaud, H., Flood, P.G., Strasser, A., 1995. Resolution Guyot (Hole 866A, Mid-Pacific Mountains): Facies Evolution and Sequence Stratigraphy. In: Winterer, E.L., Firth, J.V., Sinton, J.M. (Eds.), Proceedings O.D.P. Scientific Results, College Station, TX. 143, 133-159.

Arnaud-Vanneau, A., 2006. Biogeographic distribution of large shallow-water benthic foraminifers during the Early Cretaceous. Anuario do Instituto de Geociências 29 (1) (Forams 2006). 694 p.

Arnaud-Vanneau, A., Arnaud, H., 2005. Carbonate facies and microfacies of the Lower Cretaceous carbonate platforms. In: Adatte, T., Arnaud-Vanneau, A., Arnaud, H., BlancAlétru, M.C., Bodin, S., Carrio-Schaffhauser, E., Föllmi, K.B., Godet, A., Raddadi, M.C., Vermeulen, J. (Eds.), The Hauterivian-Lower Aptian sequence stratigraphy from Jura Platform to Vocontian Basin: A multidisciplinary approach. Géologie Alpine, Série Spéciale “Colloques et Excursions” 7, 39-68.

Arnaud-Vanneau, A., Premoli Silva, I., 1995. Biostratigraphy and systematic description of benthic foraminifers from Mid-Cretaceous shallow-water carbonate platform sediments at Site 878 and 879 (Mit and Takuyo-Daisan Guyots). In: Haggerty, J.A., Premoli Silva, I., Rack, F., McNutt, M.K. (Eds.), Proceedings O.D.P. Scientific Results, College Station, TX. 144, 199-219.

Arnaud-Vanneau, A., Sliter, W.V., 1995. Early Cretaceous shallow-water benthic foraminifers and fecal pellets from Leg 143 compared with coeval faunas from the Pacific

Basin, Central America, and the Tethys. In: Winterer, E.L., Sager, W.W., Firth, J.V., Sinton, J.M. (Eds.), Proceedings O.D.P. Scientific Results, College Station, TX. 143, 537-564.

Bagheri, S., 2007. The exotic Paleo-Tethys terrane in Central Iran: new geological data from Anarak, Jandag and posht-e-Badam areas, Ph.D. thesis, University of Lausanne, Lausanne, Switzerland. 223 pp.

Bagheri, S., Stampfli, G.M., 2008. The Anarak, Jandaq and Posht-e-Badam metamorphic complexes in central Iran: New geological data, relationships and tectonic implications. Tectonophysics 451, 123-155.

Bandel, K., 1990. Shell structure of the gastropoda excluding Archaeogastropoda, - in Skeletal Biomineralization: Patterns Processes and Evolutionary Trends. Van Nostrand, New York, v. I, Carter, J.G. (Eds.), pp. 117-134.

Barragan-Manzo, R., Diaz-Otero, C., 2004. Analisis de microfacies y datos micropaleontologicos de la transicion Barremiano-Aptiano en la Sierra de Rosario, Durango, Mexico. Revista Mexicana de Ciencias Geologicas 21, 247-259.

Berberian, M., King, G.C.P., 1981. Toward a palaeogeography and tectonic evolution of Iran. Canadian Journal of Earth Science 18, 210-265.

Bodin, S., Godet, A., Föllmi, K.B., Vermeulen, J., Arnaud, H., Strasser, A., Fiet, N., Adatte, T., 2006a. The late Hauterivian Faraoni oceanic anoxic event in the western Tethys: Evidence from phosphorus burial rates. Palaeogeography, Palaeoclimatology, Palaeoecology 235, 245-264.

Bodin, S., Godet, A., Vermeulen, J., Linder, P., Föllmi, K.B., 2006b. Biostratigraphy, sedimentology and sequence stratigraphy of the latest Hauterivian- Early Barremian drowning episode of the Northern Tethyan margin (Altmann Member, Helvetic nappes, Switzerland). Ecologae Geologicae Helvetiae 99, 157-174.

Bodrogi, I., 1999. Urgon limestone of inverse position in the SE foreland of the Villány Mts, Transdanubia, Hungary. Annual Reports of the Geological Institute of Hungray, 1992/1993/II, pp. 27-52.

Bonvallet, L., 2015. Evolution of the Helvetic shelf (Switzerland) during the Barremian–early Aptian: paleoenvironmental, paleogeographic and paleoceanographic controlling factors. PhD thesis, University of Lausanne, Lausanne, Switzerland. 333 p.

Bonvallet, L., Arnaud-Vanneau, A., Arnaud, H., Adatte, T., Spangenberg, JE., Stein, M., Godet, A., Föllmi, KB., 2019. Evolution of the Urgonian shallow-water carbonate platform on the Helvetic shelf during the late Early Cretaceous. Sedimentary Geology 387, 18-56.

Bosellini, A., Morsilli, M., Neri, C., 1999. Long-term event stratigraphy of the Apulia Platform margin (Upper Jurassic to Eocene, Gargano, southern Italy). Journal of Sedimentary Research 69, 1241-1252.

Brunet, M.F., Korotaev, M.V., Ershov, A.V., Nikishin, A.M., 2003. The South Caspian Basin: a review of its evolution from subsidence modelling. In: Brunet, M.F., Cloetingh, S. (Eds.), Integrated Peri-Tethyan Basins Studies (Peri-Tethys Programme). Sedimentary Geology 156, 119-148.

Brunet, M.F., McCann, T., Sobel, E.R. (Eds.) 2015. Geological Evolution of Central Asian Basins and the Western Tien Shan Range. Geological Society, London, Special Publications. 427 p.

Bruni, R., Bucur, I.I., Preat, A., 2007. Uppermost Jurassic-Lower Cretaceous carbonate deposits from Fara San Martino (Maiella, Italy): biostratigraphic remarks. Studia UBB, Geologia 52 (2), 45-54.

Bucur, I.I., Majidifard, M.R., Senowbari-Daryan, B., 2013. Early Cretaceous calcareous benthic microfossils from the eastern Alborz and western Kopet Dagh (northern Iran) and their stratigraphic significance. Acta Palaeontologica Romaniae 9(1), 23-37.

Bucur, I.I., Rashidi, K., Senowbari-Daryan, B., 2012. Early Cretaceous calcareous algae from Central Iran (Taft formation, south of Aliabad, near Yazd). Facies 58, 605-636.

Canérot, J., Cugny, P., Peybernès, B., Rahali, I., Rey, J., Thieuloy, J.P., 1986. Comparative study of the lower and mid-Cretaceous sequences on different Maghrebian shelves and basins– their place in the evolution of the North African Atlantic and Neotethysian margins. Palaeogeography, Palaeoclimatology, Palaeoecology 55, 213-232.

Chartrousse, A., Masse, J.P., 1998. Offneria arabicanov. sp. (rudist, Caprinidae) de l'Aptien inférieur du Jebel Madar (Sultanat d'Oman). Cretaceous Research 19, 827-841.

Davies, G.R., Smith, Jr. L.B., 2006. Structurally controlled hydrothermal dolomite reservoir facies: An overview: AAPG Bulletin, v. 90, pp. 1641-1690.

Davoudzadeh, M., 1997. Iran. In: Moores E.M., Fairbridge R.W. (Eds.), Encyclopedia of European and Asian regional geology. Encyclopedia of Earth Sciences Series, Chapman and Hall, London, pp. 384-405.

Dini, M., Tunis, G., Venturini, S., 1998. Continental, brackish and marine carbonates from the Lower Cretaceous of Kolone–Barbariga (Istria, Croatia): stratigraphy, sedimentology and geochemistry. Palaeogeography, Palaeoclimatology, Palaeoecology 140, 245–269.

Dragastan, O., Antoniade, C., Stoica, M., 2014. Biostratigraphy and zonation of the Lower Cretaceous carbonate succession from Cernavodă-lock section, south Dobrogea, eastern part of the Moesian platform (Romania). Carpathian Journal of Earth and Environmental Sciences, v. 9, n. 1, pp. 231-260.

Emmanuel, L., Renard, M., 1993. Carbonate geochemistry (Mn, $\delta^{13}C$, $\delta^{18}O$) of the late Tithonian-Berriasian pelagic limestones of the Vocontian trough (SE France), Bull. Cent. Rech. Explor. Prod. Elf Aquitaine 17, 205-221.

Erba, E., 2006. The first 150 million years history of calcareous nannoplankton: biosphere geosphere interactions. Palaeogeography, Palaeoclimatology, Palaeoecology 232, 237-250.

Erba, E., Bartolini, A., Larson, R.L., 2004. Valanginian Weissert oceanic anoxic event. Geology 32, 149-152.

Fekete, K., Soták, J., Boorová, D., Lintnerová, O., Michalík, J., Grabowski, J., 2017. An Albian demise of the carbonate platform in the Manín Unit (Western Carpathians, Slovakia). Geologica Carpathica 68(5), 385-402.

Flügel, E., 2004. Microfacies of Carbonate Rocks- Analysis, Interpretation and Application. Springer-Verlag, Berlin, Heidelberg, New York. 976 p.

Föllmi, K.B., Bodin, S., Godet, A., Linder, P., Van de Schootbrugge, B., 2007. Unlocking paleoenvironmental information from Early Cretaceous shelf sediments in the Helvetic Alps: stratigraphy is the key! Swiss Journal of Geosciences 100, 349-369.

Föllmi, K.B., Godet, A., Bodin, S., Linder, P., 2006. Interactions between environmental change and shallow-water carbonate build-up along the northern Tethyan margin and their impact on the Early Cretaceous carbon-isotope record, Paleoceanography 21, PA4211.

Föllmi, K.B., Weissert, H., Bisping, M., Funk, H., 1994. Phosphogenesis, carbon-isotope stratigraphy, and carbonate platform evolution along the Lower Cretaceous northern Tethyan margin. Geological Society of America Bulletin, v. 106, pp. 729-746.

Gheiasvand, M., Ashouri, A.R., Aghanabati, S.A., Taherpour Khalil Abad, M., Ghaderi, A., 2018. Biostratigraphy of the Tirgan Formation in the Kopet-Dagh basin: Stratigraphic sections of the Tirgan village and Amirabad section. University of Isfahan, Stratigraphy and Sedimentology Research 74, 23-36 (In Persian, English summary).

Gheiasvand, M., Ashouri, A.R., Aghanabati, S.A., Taherpour Khalil Abad, M., Ghaderi, A., 2020. Stratigraphic distribution of shallow-water benthic foraminifera from the Lower Cretaceous Taft formation, Central Iran (Yazd Block), with evidence for the importance of hiatuses. Annales de Paléontologie 106, 13.

Gheiasvand, M., Föllmi, K.B., Arnaud-Vanneau, A., Adatte, T., Spangenberg, J., Ghaderi, A., Ashouri, A.R., 2019. New stratigraphic data for the Lower Cretaceous Tirgan Formation, Kopet-Dagh Basin, NE Iran. Arabian Journal of Geosciences 12, 15.

Godet, A., Bodin, S., Föllmi, K.B., Vermeulen, J., Gardin, S., Fiet, N., Adatte, T., Zsolt, B., Stüben, D., Van de Schootbrugge, B., 2006. Evolution of the marine stable carbon-isotope record during the Early Cretaceous: A focus on the late Hauterivian and Barremian in the Tethyan realm, Earth Planet. Sci. Lett. 242, 254-271.

Godet, A., Föllmi, K.B., Bodin, S., De Kaenel, E., Matera, V., Adatte, T., 2010. Stratigraphic, sedimentological and palaeoenvironmental constraints on the rise of the Urgonian platform in the western Swiss Jura. Sedimentology. Wiley 57(4), 1088-1125.

Godet, A., Hfaiedh, R., Arnaud-Vanneau, A., Zghal, I., Arnaud, H., Ouali, J., 2014. Aptian palaeoclimates and identification of an OAE1a equivalent in shallow marine environments of the southern Tethyan margin: Evidence from Southern Tunisia (Bir Oum Ali section, Northern Chott Chain). Cretaceous Research 48, 110-129.

González-León, C.M., 1994. Early Cretaceous tectono-sedimentary evolution of the southwestern margin of the Bisbee Basin. Revista Mexicana de Ciencias Geológicas, v. 11, n. 2, pp. 139-146.

González-León, C.M., Scott, R.W., Löser, H., Lawton, T.F., Robert, E., Valencia, V.A., 2008. Upper Aptian-Lower Albian Mural Formation: stratigraphy, biostratigraphy and depositional cycles on the Sonoran shelf, northern México. Cretaceous Research 29, 249-266.

Gradstein, F.M., Ogg, J.G., Smith, A.G., 2004. A Geologic Time Scale 2004, Cambridge Univ. Press, New York. 600 p.

Hashimoto, W., Matsumaru, K., 1971. Orbitolina from the Seberuang Cretaceous, Kalimantan Barat (West Kalimantan), Geology and Paleontology of Southeast Asia. CXLI. 14, 89-99.

Haq, B.U., Hardenbol, J. Vail, P.R., 1987. Chronology of fluctuating sea levels since the Triassic. Science 235, 1156-1167.

Hennig, S., Weissert, H., Bulot, L., 1999. C-isotope stratigraphy, a calibration tool between ammonite and magnetostratigraphy: The Valanginian-Hauterivian transition, Geol. Carpathica 50, 91-96.

Hfaiedh, R., Arnaud-Vanneau, A., Godet, A., Arnaud, H., Zghal, I., Ouali, J., Latil, J.L., Jallali, H., 2013. Biostratigraphy and palaeoenvironmental evolution of the Aptian succession at Jebel Bir Oum Ali (Northern Chain of Chotts, South Tunisia): Comparison with contemporaneous Tethyan series. Cretaceous Research 46, 177-207.

James, N.P., 1997. The cool-water carbonate depositional realm. In: James, N.P., Clarke, J.A.D. (Eds.), Cool-water Carbonates. SEPM Special Publication 56, 1-20.

Jenkyns, H.C., 2010. Geochemistry of oceanic anoxic events. Geochemistry, Geophysics, Geosystems 11, 30.

Herrle, J.O., Kößler, P., Friedrich, O., Erlenkeuser, H., Hemleben, C., 2004. High-resolution carbon isotope records of the Aptian to lower Albian from SE France and the Mazagan Plateau (DSDP Site 545), a stratigraphic tool for paleoceanographic and paleobiologic reconstruction, Earth Planet. Sci. Lett. 218, 149-161.

Hosseini, S., 2014. Holostratigraphy of the Berriasian - Aptian carbonate platform deposits from the Zagros fold-thrust belt, SW Iran. Ph.D. thesis, No 4713, University of Geneva. 253 p.

Husinec, A., Sokač, B., 2006. Early Cretaceous benthic associations (foraminifera and calcareous algae) of a shallow tropical-water platform environment (Mljet Island, southern Croatia). Cretaceous Research 27, 418-441.

Immel, H., Seyed-Emami, K., Afshar-Harb, A., 1997. Kreide-Ammoniten aus dem iranischen Teil des Koppeh Dagh (NE Iran). Zitteliana 21, 159-190.

Ivanova, D., Bonev, N., Chatalov, A., 2015. Biostratigraphy and tectonic significance of lowermost Cretaceous carbonate rocks of the Circum-Rhodope Belt (Chalkidhiki Peninsula and Thrace region, NE Greece). Cretaceous Research 52, 25-63.

Jankičević, J., 1978. Barrémien et Aptien des parties moyennes des Carpatho Balkanides dans la Serbie orientale au point de vue du developpement d'Urgonien. Geolo ski Anali Balkanskoga Poluostrva 42, 103-194. (In Serbian, French summary).

Kendall, C.G., Lerche, I., 1988. The rise and fall of eustacy. In: Wilgus, C.K., Hastings, B.S., Kendall, C.G.St.C., Posamentier, H.W., Ross, C.A., and Van Wagoner, J.C. (Eds.), Sea-Level Changes: An Integrated Approach SEPM Spec. Pub. 42, 3–18.

Kilian, W., 1907. Kreide. Erste Abteilung: Unterkreide (Paleocrretacicum): Handbuch der Erdgeschichte für die Formationen bezeichdsten Versteinerungen, von einer Vereinigung von Geologen, v. II: Stuttgart, Fritz Frech, pp. 1-108.

Kovatcheva, T., 1979. Foraminifera from the Urgonian sediments in Bulgaria and their stratigraphic significance. Geobios 3, 183-191.

Krajewski, M., Olszewska, B., 2007. Foraminifera from the Late Jurassic and Early Cretaceous carbonate platform facies of the Southern part of the Crimea mountains, southern Ukraine: Annales Societatis Geologorum Poloniae 77, 291-311.

Lesná, S., 1997. Welcome in the field trips of the IGCP project 362 final meeting. Mineralia Slovaca 29, 357-383.

Loeblich, A.R. Jr., Tappan, H., 1988. Foraminiferal Genera and their classification: Van Nostrand Reinhold. New York. 847 p.

Longoria, J.F., 1972. Stratigraphic, morphologic and taxonomic studies of Aptian planktonic Foraminifera. PhD thesis, The University of Texas, Dallas. 478 p.

Longoria, J.F., 1973. On the stratigraphic distribution of the Tintinnid genus Colomiella. Soc. Geol. Mexicana. Bol. 34, 97-99.

Longoria, J.F., Gamper, M.A., 1974. Albian planktonic foraminifera from the Sabinas Basin of Northern Mexico. VI African Colloquium of Micropaleontology. Tunisia 28, 39-71.

Machel, H.G., 2004. Concepts and models of dolomitization: a critical reappraisal. In: Braithwaite, C.J.R., Rizzi, G., Darke, G. (Eds.), The geometry and petrogenesis of dolomite hydrocarbon reservoirs: Geological Society (London). Special Publications, v. 235, pp. 7-63.

Mancinelli, A., Chiocchini, M., 2006. Cretaceous benthic foraminifers and calcareous algae from Monte Cairo (southern Latium, Italy). Bollettino della Società Paleontologica Italiana 45(1), 91-113.

Martin, U., Breitkreuz, C., Egenhoff, S., Enos, P., Jansa, L., 2004. Shallow-marine phreatomagmatic eruptions through a semi-solidified carbonate platform (ODP Leg 144, Site 878, Early Cretaceous, MIT Guyot, West Pacific). Marine Geology 204, 251-272

Masse, J.P., Tüysüz, O., Fenerci-Masse, M., Özer, S., Sari, B., 2009b. Stratigraphic organisation, spatial distribution, palaeoenvironmental reconstruction, and demise of Lower Cretaceous (Barremian-lower Aptian) carbonate platforms of the Western Pontides (Black Sea region, Turkey). Cretaceous Research 30, 1170-1180.

Masse, J.P., Villeneuve, M., Leonforte, E., Nizou, J., 2009a. Block tilting of the North Provence Early Cretaceous carbonate margin: stratigraphic, sedimentologic and tectonic data. Bull. Soc. Geol. France 180, 105-115.

Matrion, B., 2010. Les ammonites. In: Colleté, C. (Eds.), Stratotype de l'Albien. Publications Scientifiques du Muséum, Paris, Collection "Patrimoine géologique"; Biotope Editions, Mèze; Brgm Editions, Orléans, pp. 99-193.

Matsumaru, K., 2005. *Praeorbitolinoides*, a new Orbitolinid foraminiferal genus from the Lower Aptian (Cretaceous) of Hokkaido, Japan. Micropaleontology 51, 93-99.

Mehrnusch, M., 1973. Eine Orbitoliniden-Fauna aus der Unterkreide von Esfahan (Zentral-Iran). N Jb Geol Paläont Mh. 6, 374-382.

Michel, J., Borgomano, J., Reijmer, J.J.G., 2018. Heterozoan carbonates: When, where and why? A synthesis on parameters controlling carbonate production and occurrences. Earth-Science Reviews 182, 50-67.

Monreal, R., Longoria, J.F., 2000. Lower Cretaceous rocks of Sierra Los Chinos, east-central Sonora, Mexico. Geofísica Internacional, v. 39, n. 4, pp. 309-322.

Morsilli, M., Hairabian, A., Borgomano, J., Nardon, S., Adams, E.W., Bracco Gärtner, G.L., 2017. The Apulia Carbonate Platform in the Gargano Promontory (Upper Jurassic To Eocene - Southern Italy). Am. Assoc. Pet. Geol. Bull. 4, 523–531.

Moullade, M., Kuhnt, W., Bergen, J.A., Masse, J.P., Tronchetti, G., 1998. Correlation of biostratigraphic and stable isotope events in the Aptian historical stratotype of La Bedoule (southeast France), C. R. Acad. Sci., Ser. IIa Sci. Terre Planetes 327, 693-698.

Neagu, Th., 1997. Lower Cretaceous agglutinated Foraminifera from the superfamilies Verneuilinacea and Ataxophragmiacea; southern Dobrogea, Romania. Annales Societatis Geologorum Poloniae 67, 307-323.

Neagu, Th., Cîrnaru, P., 2002. New species of *Ammomarginulina* and *Feurtillia* in the Lower Cretaceous deposits from Cernavoda-Aliman area, Southern Dobrogea, Romania. Studia Universitatis Babes-Bolyai, Geologia, v. 1, pp. 245-254.

Ogg, J.G., 1995. MIT Guyot; depositional history of the carbonate platform from downhole logs at Site 878 (lagoon). In: Haggerty, J., Premoli Silva, I., Rack, F., McNutt, M.K. (Eds.), Proceedings O.D.P. Scientific Results, College Station, TX. 144, 337-359.

Omana-Pulido, L., Pantoja-Alor, J., 1998. Early Aptian benthic foraminifera from the El Cajon formation, Huetamo, Michoacan, SW Mexico. Revista Mexicana de Ciencias Geologicas 15, 64-72.

Peybernès, B., 1979. L'urgonien de Hongrie. Géobios 12, sup.1, 231-243.

Picotti, V., Cobianchi, M., Luciani, V., Blattmann, F, Schenker, T., Mariani, E., Bernasconi, S., Weissert, H., 2019. Change from rimmed to ramp platform forced by regional and global events in the Cretaceous of the Friuli-Adriatic Platform (Southern Alps, Italy). Cretaceous Research 104, 20.

Poroshina, L.A., 1976. The new genus Conorbinella (foraminifera) from the lower Cretaceous deposits of northeatern Azerbaidjan. Questions of Stratigraphy and Paleontology Azerbaijan 1, 109-113.

Pudsey, C., Schroeder, R. and Skelton, P.W., 1985. Cretaceous (Aptian/Albian) age for island arc volcanics, Kohistan, N. Pakistan. In: Gupta, V. J. (Eds.), Geology of Western Himalayas, Contributions to Himalayan Geology 3, 150-168.

Rameil, N., Immenhauser, A., Warrlich, G., Hillgärtner, H., Droste, H.J., 2010. Morphological patterns of Aptian *Lithocodium–Bacinella* geobodies: relation to environment and scale. Sedimentology 57, 883-911.

Reháková, D., Michalík, J., Ožvoldová, L., 1996. New microbiostratigraphical data from several Lower Cretaceous pelagic sequences of the northern calcareous Alps, Austria (preliminary results). Geol. Palaönt. Mitt. Innsbruck 4, 57-81.

Riccardi, A.C., 1991. Jurassic and Cretaceous marine connections between the Southeast Pacific and Tethys. Palaeogeography, Palaeoclimatology, Palaeoecology 87, 155-189.

Robert, A., Kavoosi, M.A., Sherkati, Sh., Müller, C., Vergés, J., Aghababaei, A., 2014. Structural evolution of the Kopet Dagh fold-and-thrust belt (NE Iran) and interactions with the South Caspian Sea Basin and Amu Darya Basin. Marine and Petroleum Geology 57, 68-87.

Schlagintweit, F., 2011. The dasycladalean algae of the Plassen carbonate platform (Kimmeridgian-Early Berriasian): taxonomic inventory and palaeogeographical implications

within the platform-basin system of the Northern Calcareous Alps (Austria, p.p. Germany). Geologia Croatica 64 (3), 185-206.

Schlagintweit, F., Rosales, L., Najarro, M., 2016. *Glomospirella cantabrica* n. sp., and other benthic foraminifera from Lower Cretaceous Urgonian-type carbonates of Cantabria, Spain: Biostratigraphic implications. Geologica Acta 14, 113-138.

Schlanger, S.O., Jenkyns, H.C., 1976. Cretaceous Oceanic Anoxic Events: causes and consequences. Geologie en Mijnbouw 55, 179-184.

Scholle, P.A., Umer-Scholle, D.S., 2003. A color guide to the petrography of carbonate rocks: grains, textures, porosity, diagenesis. American Association of Petroleum Geology, Memoir 77, Tulsa, Oklahoma. 459 p.

Schroeder, R., 1965. *Dictyoconus pachymarginalis* n. sp. aus dem Apt des Elburz- Gebirges (Nord-Iran) (Studien über primitive Orbitolinidae III). Eclogae Geologicae Helvetiae 58, 976-979.

Seyed-Emami, K., Immel, H., 1995. Ammoniten aus dem Alb (Kreide) von Shir-Kuh (N Yazd, Zentraliran). Paläontäontologische Zeitschrift 69, 377-399.

Siehl, A., 2017. Structural setting and evolution of the Afghan orogenic segment – a review. Geological Society, London, Special Publications 427, issue 1, pp. 57-88.

Skelton, P.W., Gili, E., 2012. Rudists and carbonate platforms in the Aptian: a case study on biotic interactions with ocean chemistry and climate. Sedimentology 59, 81-117.

Spangenberg, J.E., Bagnoud-Velásquez, M., Boggiani, P.C., Gaucher, C., 2014. Redox variations and bioproductivity in the Ediacaran: Evidence from inorganic and organic geochemistry of the Corumbá Group, Brazil. Gondwana Research 26, 1186-1207.

Stampfli, G.M., 2000. Tethyan oceans. In: Bozkurt, E., Winchester, J.A., Piper, J.D.A. (Eds.), Tectonics and Magmatism in Turkey and Surrounding Area. Geological Society of London, Special Publication 173, 1-23.

Stampfli, G.M., Borel, G.D., 2004. The Transmed transects in space and time: constraints on the paleotectonic evolution of the Mediterranean domain. In: Cavazza, W., Roure, F.M., Spakman, W., Stampfli, G.M., Ziegler, P.A. (Eds.), The Transmed Atlas-The Mediterranean region from crust to mantle. Springer, Berlin, pp. 53-80.

Stampfli, G.M., Kozur, H.W., 2007. Europe from the Variscan to the Alpine cycles. In: Gee, D.G., Stephenson, R. (Eds.), European Lithosphere Dynamics. Memoir of the Geological Society (London), pp. 57-82.

Stampfli, G.M., Marcoux, J., Baud, A., 1991. Tethyan margins in space and time. In: Channell, J.E.T., Winterer, E.L., Jansa, L.F. (Eds.), Paleogeography and Paleoceanography of Tethys. Palaeogeography, Palaeoclimatology, Palaeoecology 87, 373-410.

Stampfli, G.M., Mosar, J., Favre, P., Pillevuit, A., Vannay, J.-C., 2001. Permo- Mesozoic evolution of the western Tethyan realm: the Neo-Tethys/East- Mediterranean connection. In: Ziegler, P.A., Cavazza, W., Robertson, A.H.F., Crasquin-Soleau, S. (Eds.), PeriTethys Memoir 6: Peritethyan Rift/Wrench Basins and Passive Margins, IGCP 369. Mém. Museum Nat. Hist. Nat, Paris, pp. 51-108.

Stein, M., Westermann, S., Adatte, T., Matera, V., Fleitmann, D., Spangenberg, J.E., Föllmi, K.B., 2012. Late Barremian–Early Aptian palaeoenvironmental change: The Cassis-La Bédoule section, southeast France: Cretaceous Research 37, 209-222.

Steuber, T., 2002. Plate tectonic control on the evolution of Cretaceous platform-carbonate production. Geology 30, 259-262.

Stöcklin, J., 1968. Structural history and tectonics of Iran: a review. The American Association of Petroleum Geologists Bulletin 52 (7), 1229-1258.

Sudar, M., Jovanovi, D., Maran, A., Polavder, S., 2008. Late Barremian–Early Aptian Urgonian limestones from the south-eastern Kučaj Mountains (Carpatho-Balkanides, eastern Serbia). Annales Géologiques de la Péninsule Balkanique 69, 13-30.

Takin, M., 1972. Iranian geology and continental drift in the Middle East. Nature 23, 147-150.

Tawadros, E., 2011. Geology of North Africa. CRC Press. 390 p.

Tennant, J.P., Mannion, P.D., Upchurch, P., Sutton, M.D., Price, G.D., 2016. Biotic and environmental dynamics through the Late Jurassic–Early Cretaceous transition: evidence for protracted faunal and ecological turnover. Biological Reviews of the Cambridge Philosophical Society 92(2), 776-814.

Trejo M., 1975. Zonificación del límite Aptiano-Albiano de México. Rev. Inst. Mex. Petrol., v. VII, 5, 6-19.

Van Buchem, F.S.P., Pittet, B., Hillgärtner, H.A., Al-Mansouri, A., Billing, I., Droste, H., Grötsch, J., Oterdoom, H., 2002. Regional sequence stratigraphic model for the Kharaib and Shuaiba Formations (Barremian, Aptian) in N. Oman and the UAE – depositional geometries and ecological change. GeoArabia 7, 461-500.

Van de Schootbrugge, B., Föllmi, K.B., Bulot, L.G., Burns, S.J., 2000. Paleoceanographic changes during the early Cretaceous (Valanginian-Hauterivian): Evidence from oxygen and carbon stable isotopes, Earth Planet. Sci. Lett. 181, 15-31.

Vasković, N., Jović, V., Matović, V., 2010. Early Cretaceous glauconite formation and Late Cretaceous magmatism and metallogeny of the East Serbian part of the Carpatho-Balkanides. Acta Mineralogica-Petrographica, Field guide series 25, 1-32.

Velić, I., 2007. Stratigraphy and Paleobiogeography of Mesozoic Benthic Foraminifera of the Karst Dinarides (SE Europe). Geologica Croatica 60, 1-114.

Vérard, C., 2018. Panalesis: towards global synthetic palaeogeographies using integration and coupling of manifold models. Geological Magazine 156, 1-11.

Vilas, L., Masse, J.P., Arias, C., 1995. Orbitolina episodes in carbonate platform evolution: the early Aptian model from SE Spain. Palaeogeography, Palaeoclimatology, Palaeoecology 119, 35-45.

Voznesenskii, A., Gorbachik, T., Kuznetsova, K., 2002. Jurassic and Cretaceous Sea basins in the Southeastern part of the Lesser Caucasus: Sedimentation Settings and Foraminiferal Assemblages. Stratigraphy and Geological Correlation 10 (3), 53-66 (in Russian).

Weissert, H., Lini, A., Föllmi, K.B., Kuhn, O., 1998. Correlation of early Cretaceous carbon isotope stratigraphy and plate-form drowning event: a possible link? Palaeogeography, Palaeoclimatology, Palaeoecology 137, 189-203.

Westermann, S., Caron, M., Fiet, N., Fleitmann, D., Matera, V., Adatte, T., Föllmi, K.B., 2010. Evidence for oxic conditions during oceanic anoxic event 2 in the northern Tethyan pelagic realm. Cretaceous Research 31, 500-514.

Westermann, S., Duchamp-Alphonse, S., Fiet, N., Fleitmann, D., Matera, V., Adatte, T., Föllmi, K.B., 2013. Paleoenvironmental changes during the Valanginian: new insights from variations in phosphorus contents and bulk- and clay mineralogies in the western Tethys. Palaeogeography, Palaeoclimatology, Palaeoecology 392, 196-208.

Wilmsen, M., Berensmeier, M., Fürsich, F.T., Majidifard, M.R., Schlagintweit, F., 2018. A Late Cretaceous epeiric carbonate platform: the Haftoman Formation of Central Iran. Facies 64 (2), 11.

Wilmsen, M., Fürsich, F.T., Majidifard, M.R., 2013. The Shah Kuh Formation, a latest Barremian – Early Aptian carbonate platform of Central Iran (Khur area, Yazd Block). Cretaceous Research 39, 183-194.

Wilmsen, M., Fürsich, F.T., Majidifard, M.R., 2015. An overview of the Cretaceous stratigraphy and facies development of the Yazd Block, western Central Iran. Journal of Asian Earth Sciences 102, 73-91.

Wilmsen, M., Fürsich, F.T., Seyed-Emami, K., Majidifard, M.R., Taheri, J., 2009. The Cimmerian Orogeny in northern Iran: tectonostratigraphic evidence from the foreland. Terra Nova. 21, 211-218.

Winterer, E.L., Natland, J.H., Van Waasbergen, R.J., Duncan, R.A., McNutt, M.K., Wolfe, C.J., Premoli Silva, I., Sager, W.W., Sliter, W.V., 1993. Cretaceous guyots in the north-west Pacific: An overview of their geology and geophysics. In: Pringle, M.S., Sager, W.W., Sliter, W.V., Stein, S. (Eds.), The Mesozoic Pacific: Geology, Tectonics, and Volcanism. Geophysical Monograph, American Geophysical Union, Washington, DC, pp. 307-334.

Yavarmanesh1, H., Vaziri, S.H., Aryaei, A.A., Jahani, D., Pourkermani, M., Khademi Bouriabadi, E., 2017. Benthic foraminiferal and calcareous algae assemblages in the Tirgan Formation (urgonien facies type) in south flank of Ghorogh syncline (north of Chenaran), NE Iran. Open Journal of Geology 7, 796-805.

Zghal, I., Bismuth, H., Razgallah, S., Damotte, R., Ben Hadjali, N., 1996. Biostratigraphie de l'Albien du Koudiat el Beida (Nord du J. Mrhila, Tunisie centrale). In: Géologie Méditerranéenne 23, 27-61.

FIGURE CAPTIONS

Fig. 1: Schematic settings of the Kopet-Dagh basin and Yazd Block during **a**) the Late Triassic; **b**) the Mid-Jurassic; **c**) the Late Cretaceous and **d**) the Mid-Paleogene (modified from Robert et al., 2014).

Fig. 2: (**a**). Simplified structural map of Iran (modified from Wilmsen et al., 2009; see also Gheiasvand et al., 2018, 2019, 2020), with indications of the location of the investigated sections in the Kopet-Dagh mountain range and Yazd Block; **b**) KD sections; **c**) YB sections.

Fig. 3: Lithology and microfacies of the studied sections in the Kopet-Dagh basin and Yazd Block (Tirgan village section is after Gheiasvand et al., 2019). l: lower; u: upper; Be: Berriasian; Va: Valanginian; Ha: Hauterivian; Ba: Barremian; Ap: Aptian; Al: Albian.

Fig. 4: The Tirgan Fm in the Padeha section, and the contacts with the underlying Shourijeh Fm and overlying Sarcheshmeh Fm.

Fig. 5: Distribution of main microfacies along a rimmed platform and microphotographs of them (B, G and J are after Gheiasvand et al., 2019), in addition to evidence of dolomitisation (D). **A**: pelagic facies (F1, 26 m); **B**: echinoid facies (F2, 614 m); **C**: annelid facies (F3a, 10 m); **D**: calcareous sponge facies (F4, 508 m); **E**: bryozoan facies (F4, 321 m); **F**: foraminiferal facies with rounded debris (F5, 125 m); **G**: oolitic facies (F6, 285 m); **H**: coral facies (F7, 14 m); **I**: miliolid facies (F8, 109 m); **J**: oncolite facies (F10, 169 m); **K**: supralittoral facies (F11b, 407.5 m); **L**: dolomitized limestone (D, 38 m).

Fig. 6: (**a**). Lithology, whole-rock carbon and oxygen isotope record, and phosphorus content through the studied sections in the Kopet-Dagh basin (Tirgan village section is after Gheiasvand et al., 2019). (**b**). Chronostratigraphy of the Tirgan Fm in this study. For legends and abbreviations, see Figs. 3.

Fig. 7: Lithology, whole-rock carbon and oxygen isotope record, and phosphorus content through the studied sections in Yazd Block (Tirgan village section is after Gheiasvand et al., 2019). (**b**). Chronostratigraphy of the Taft fm in this study. mid: middle (For the other abbreviations and legends, see Figs. 3).

Fig. 8: Distribution of index microfossils on the plate tectonic maps from the Panalesis model (Vérard, 2018) at **a**) 140 Ma; **b**) 130 Ma; and **c**) 120 Ma., with faunal migration routes. According to the distribution of the Early Cretaceous benthic foraminifera and colomiellids and also settings of the paleogeographic clusters, six faunal provinces (northern Neotethys,

southern Neotethys, southern Alpine Tethys, northern Alpine Tethys, Gulf of Mexico and northern Pacific Ocean) are defined.

Fig. 9: Correlation between the bulk-rock $\delta^{13}C$ record from the sections of the Kopet-Dagh basin and Yazd Block and a reference record from southeastern France (Föllmi, et al., 2006; Gheiasvand et al., 2019). e: early; mid: middle; l: late. 1. stages and substages; 2. ammonite zones; 3. calpionellid zones; 4. planktonic foraminiferal zones; 5. calcareous nannoplankton zones; and 6. oceanic anoxic events (Gradstein et al., 2004).

Fig. 10: Lithostratigraphic units in the main zones of Iran (from Berriasian to Albian; modified from Immel et al., 1997 and Aghanabati and Rezaee, 2009). l: lower; u: upper.

Fig. 11: Paleogeographic reconstruction of the northern margin of Neotethys during the late Oxfordian (Panalesis model; Vérard, 2018) showing the location of the Farah and south Caspian back-arc basins. A-T: Alpine Tethys; ANAT: Anatolia; AFGH.: Afghanistan; IZANCA: Izmir Ankara; SS: Sanandaj Sirjan; Al: Alborz; Kd: Kopet-Dagh; Ya: Yazd Block; Tb: Tabas Block; Lu: Lut Block. For some legends, see Figs. 8.

Fig. 12: (**a**). The studied sections with the disappearance of the Tirgan Fm in the eastern part of the Kopet-Dagh mountain range as seen on Google Earth. (**b**). The lateral extension of the successions of the Tirgan Fm and the onlap contacts with the underlying Shourijeh Fm and overlying Sarcheshmeh Fm in the type area. (**c**). The highest parts of the Tirgan Fm with onlap deposits onto a paleovalley in the setting of the Tirgan village section.

Fig. 13: (**a**). Google Earth image of the lateral extension of the sedimentary strata of the Taft fm, and the contacts with the underlying Sangestan fm and overlying Darreh-Zanjir fm (**b**). The studied sections in the Yazd Block.

Fig. 14: (**a**). The Amirabad section with evidence of emersion below the red bed (paleosol; description of the units is in Gheiasvand et al., 2018). (**b**). microscopic aspect of the karstification (microcaves, scale; 200 μm).

Fig. 15: Scatter plots of $\delta^{13}C$ vs. $\delta^{18}O$ from the sections of Tirgan village, Amirabad, Padeha and Tamer. The coloured squares show the associations of microfacies (MF1 to MF3).

Fig. 16: Evolution of the phosphorus content vs. percent of the effective allochems through the studied sections in the Kopet-Dagh mountain range and Yazd Block.

TABLE CAPTIONS

Table 1: Summary of main microfacies of the studied Lower Cretaceous successions along a rimmed platform (Based on the Arnaud-Vanneau and Arnaud (2005) classification).

Table 2: Summary of biostratigraphic records through stratigraphic sections in the Kopet-Dagh basin and Yazd Block. Marker microfossils are highlighted (e: early; l: late; Va: Valanginian; Ha: Hauterivian; Ba: Barremian; Ap: Aptian; Al: Albian).

Table 3: List of microfossils and reported localities at 140 Ma (e: early; l: late; Be: Berriasian; Va: Valanginian; Ha: Hauterivian).

Table 4: List of microfossils and reported localities at 130 Ma (e: early; l: late; Be: Berriasian; Va: Valanginian; Ha: Hauterivian; Ba: Barremian).

Table 5: List of microfossils and reported localities at 120 Ma (e: early; l: late; Ha: Hauterivian; Ba: Barremian; Ap: Aptian; Al: Albian).

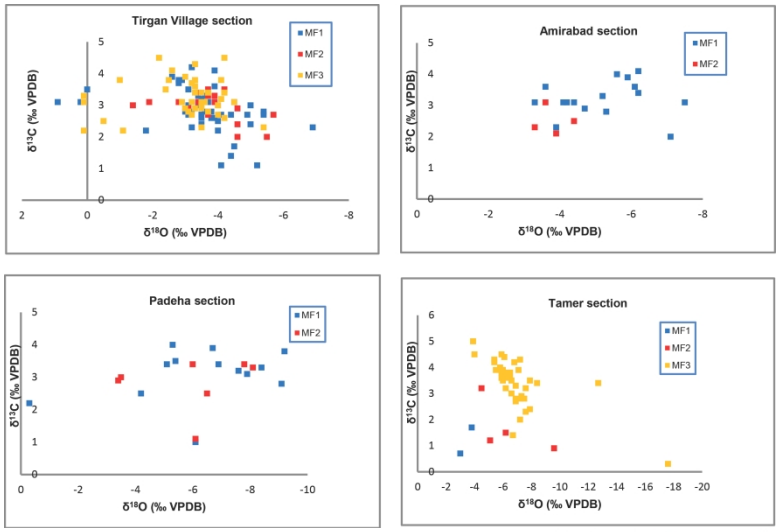

36°33′40″N; 60°04′02″E

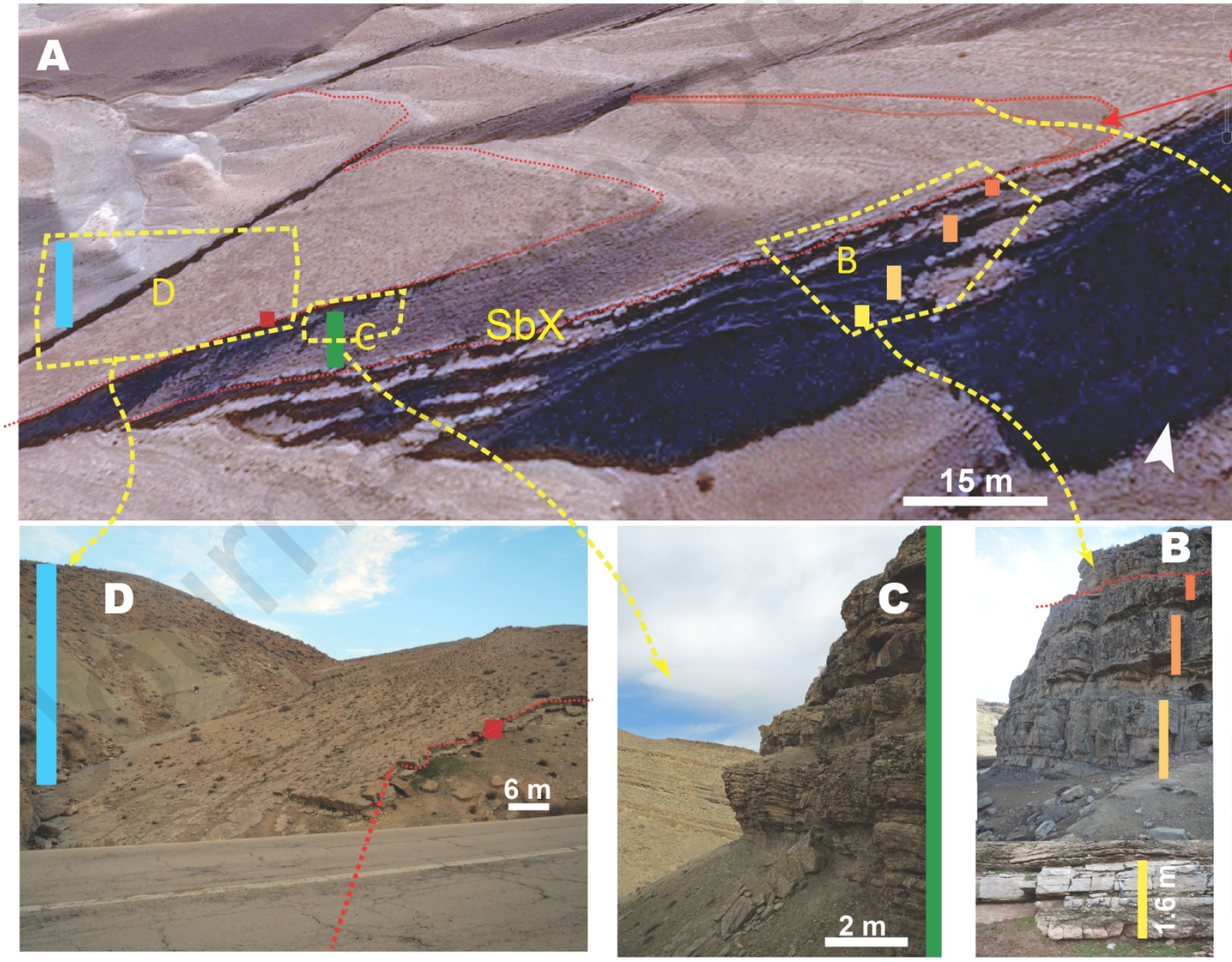

(a)

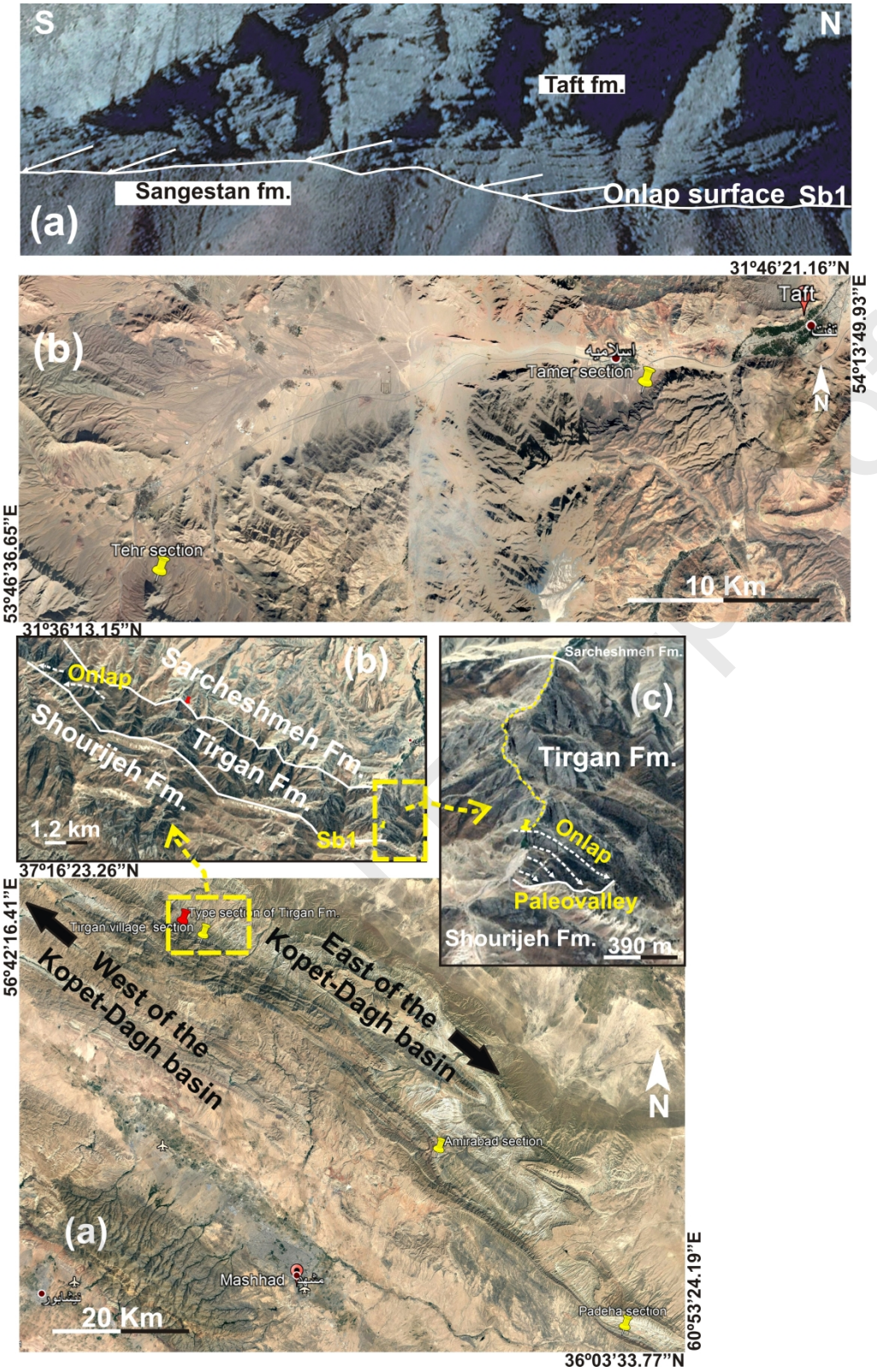
S
N
Taft fm.
Sangestan fm.
Onlap surface Sb1
(a)
31°46'21.16"N
(b)
Taft
Tamer section
N
54°13'49.93"E
Tehr section
10 Km
53°46'36.65"E
31°36'13.15"N
Onlap
Sarcheshmeh Fm.
Tirgan Fm.
Shourijeh Fm.
1.2 km
Sb1
37°16'23.26"N
(b)
Sarcheshmen Fm.
(c)
Tirgan Fm.
Onlap
Paleovalley
Shourijeh Fm.
390 m
56°42'16.41"E
Type section of Tirgan Fm.
Tirgan village section
West of the Kopet-Dagh basin
East of the Kopet-Dagh basin
N
Amirabad section
(a)
Mashhad
20 Km
Padeha section
60°53'24.19"E
36°03'33.77"N

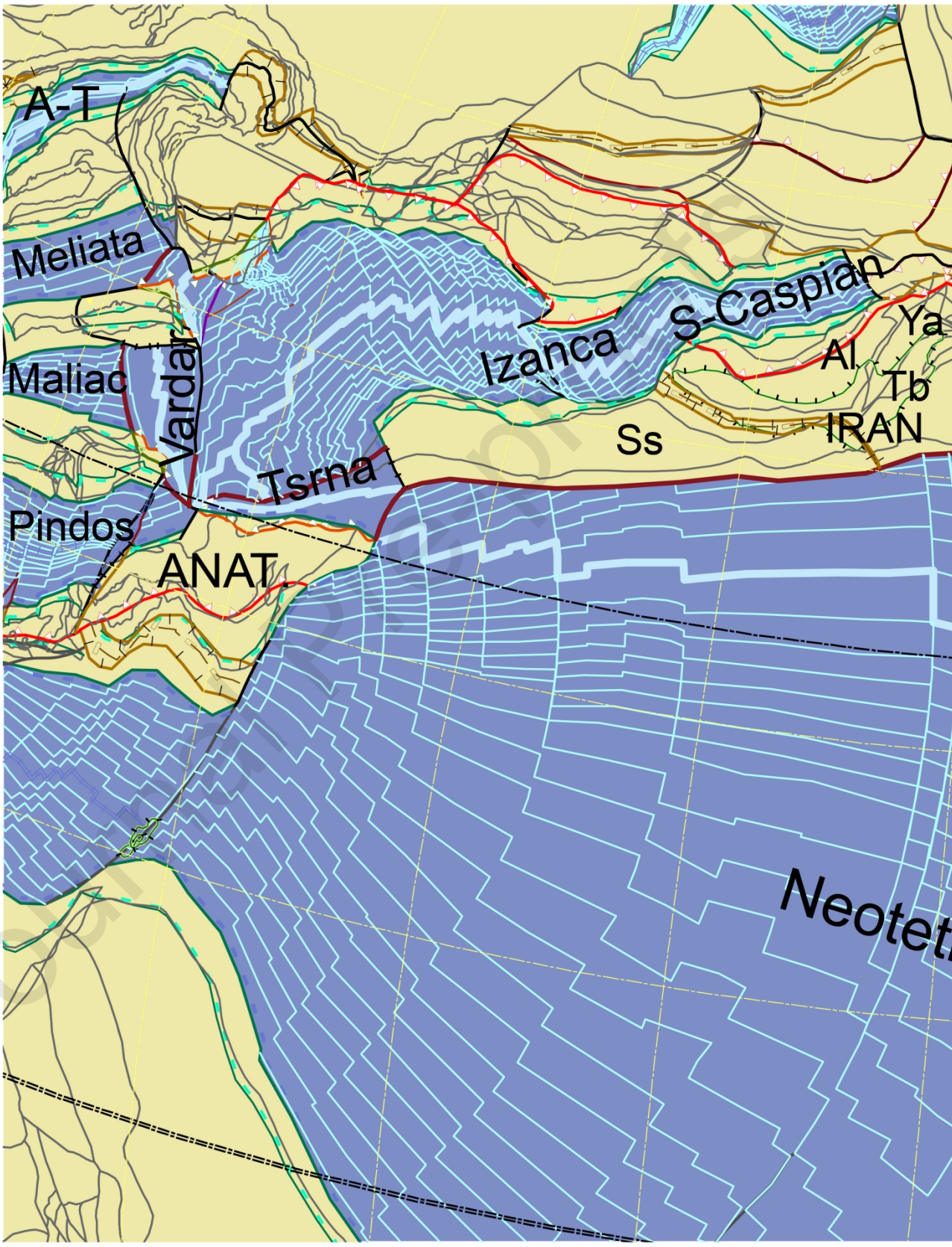

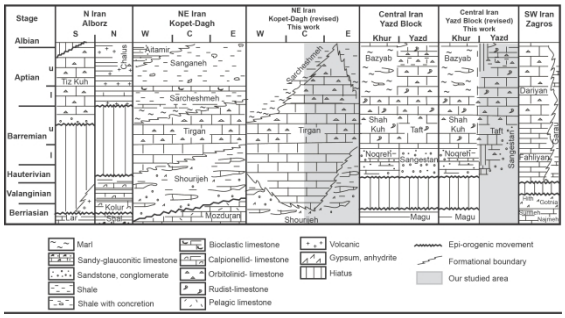

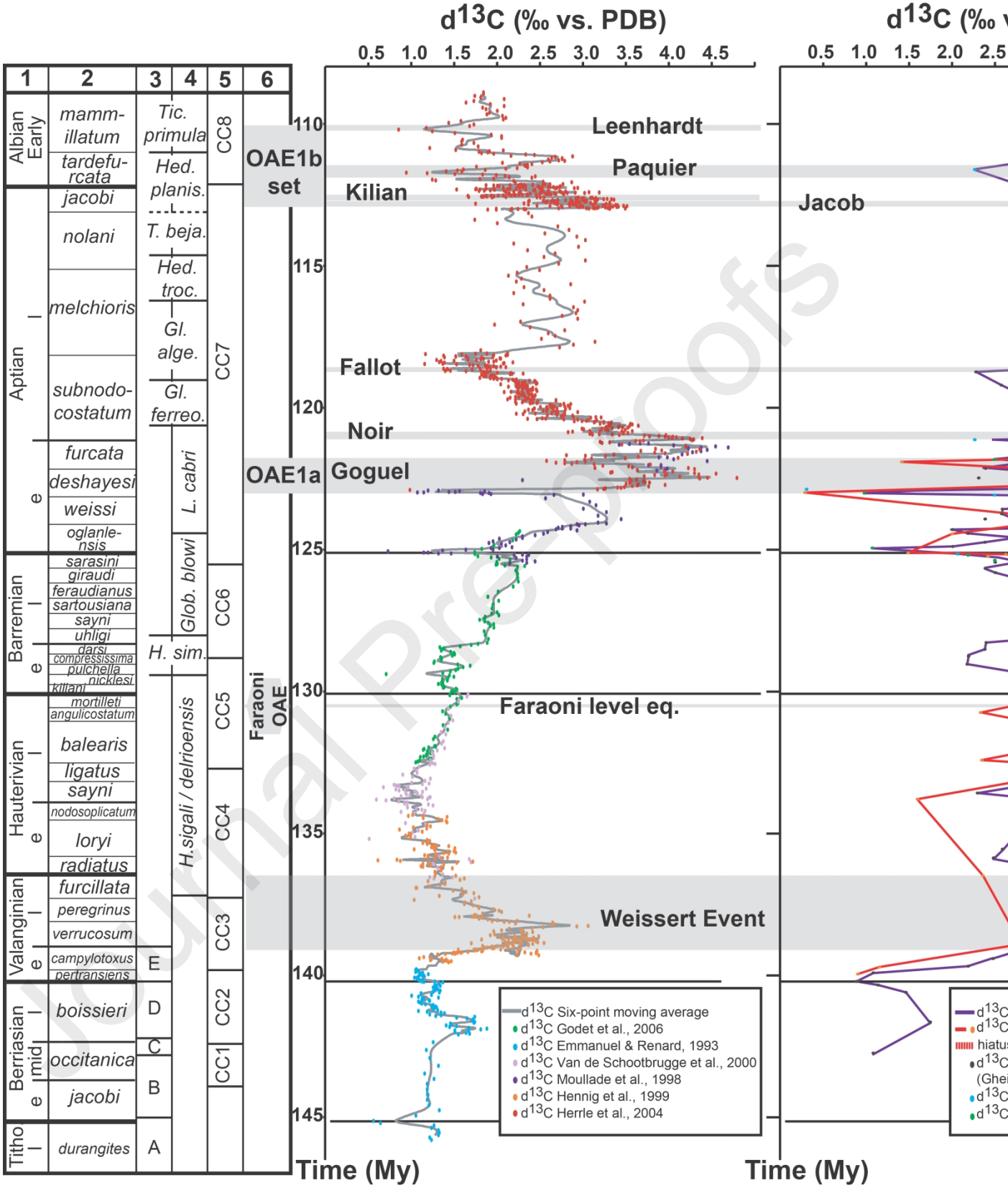

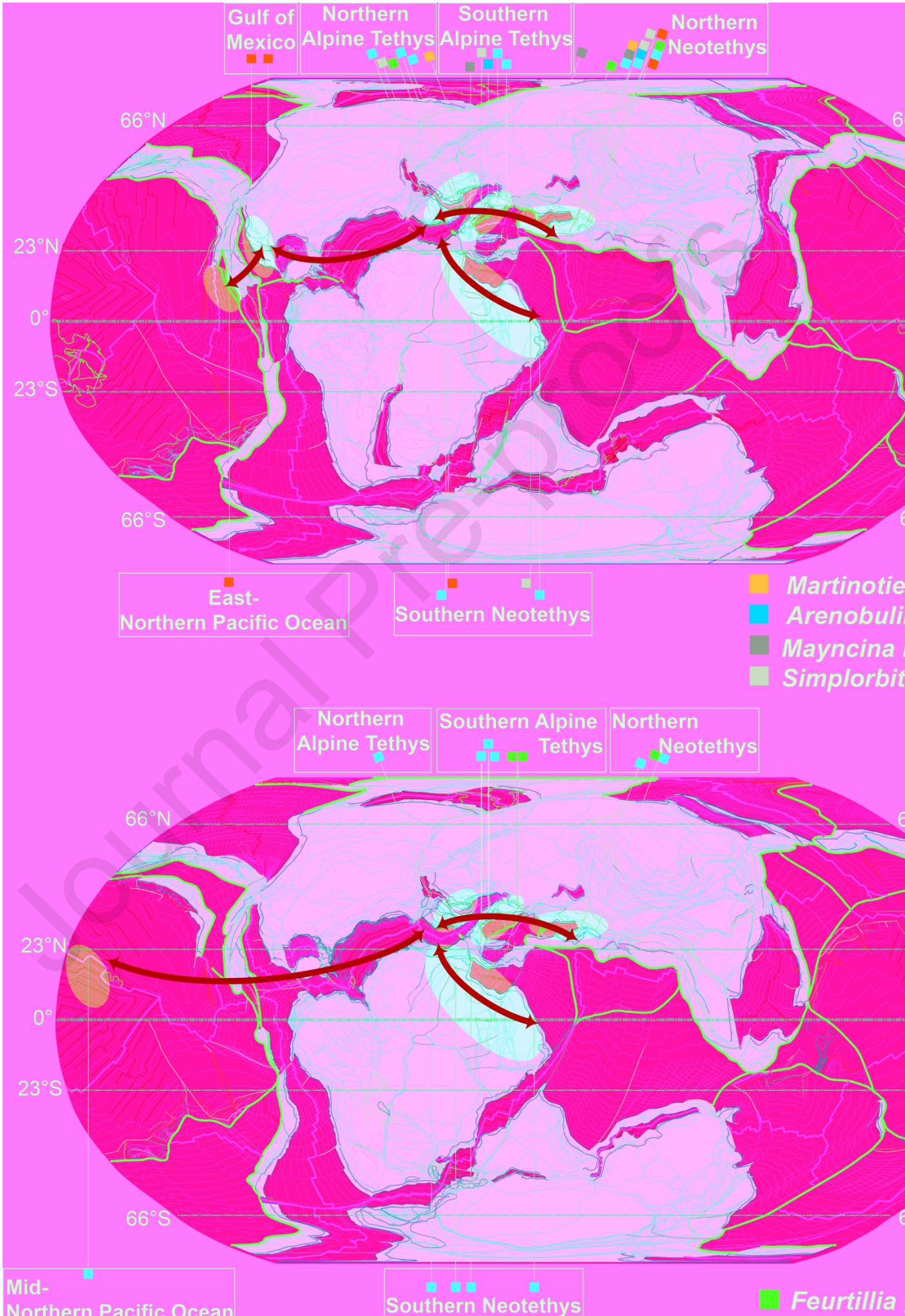
Gulf of Mexico
Northern Alpine Tethys
Southern Alpine Tethys
Northern Neotethys
66°N
23°N
0°
23°S
66°S
East-Northern Pacific Ocean
Southern Neotethys
Martinotie
Arenobuli
Mayncina
Simplorbit
Northern Alpine Tethys
Southern Alpine Tethys
Northern Neotethys
66°N
23°N
0°
23°S
66°S
Mid-Northern Pacific Ocean
Southern Neotethys
Feurtillia

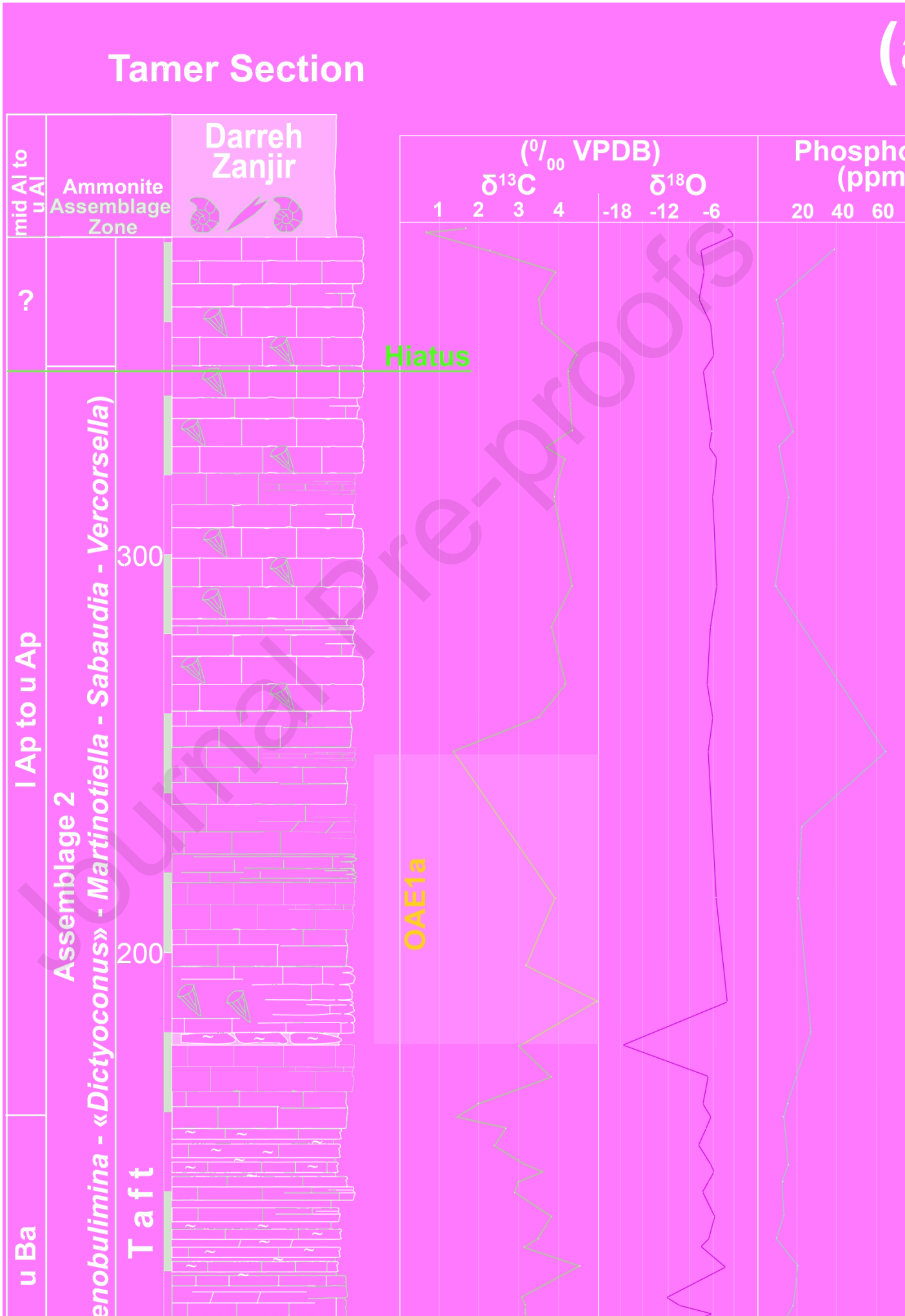

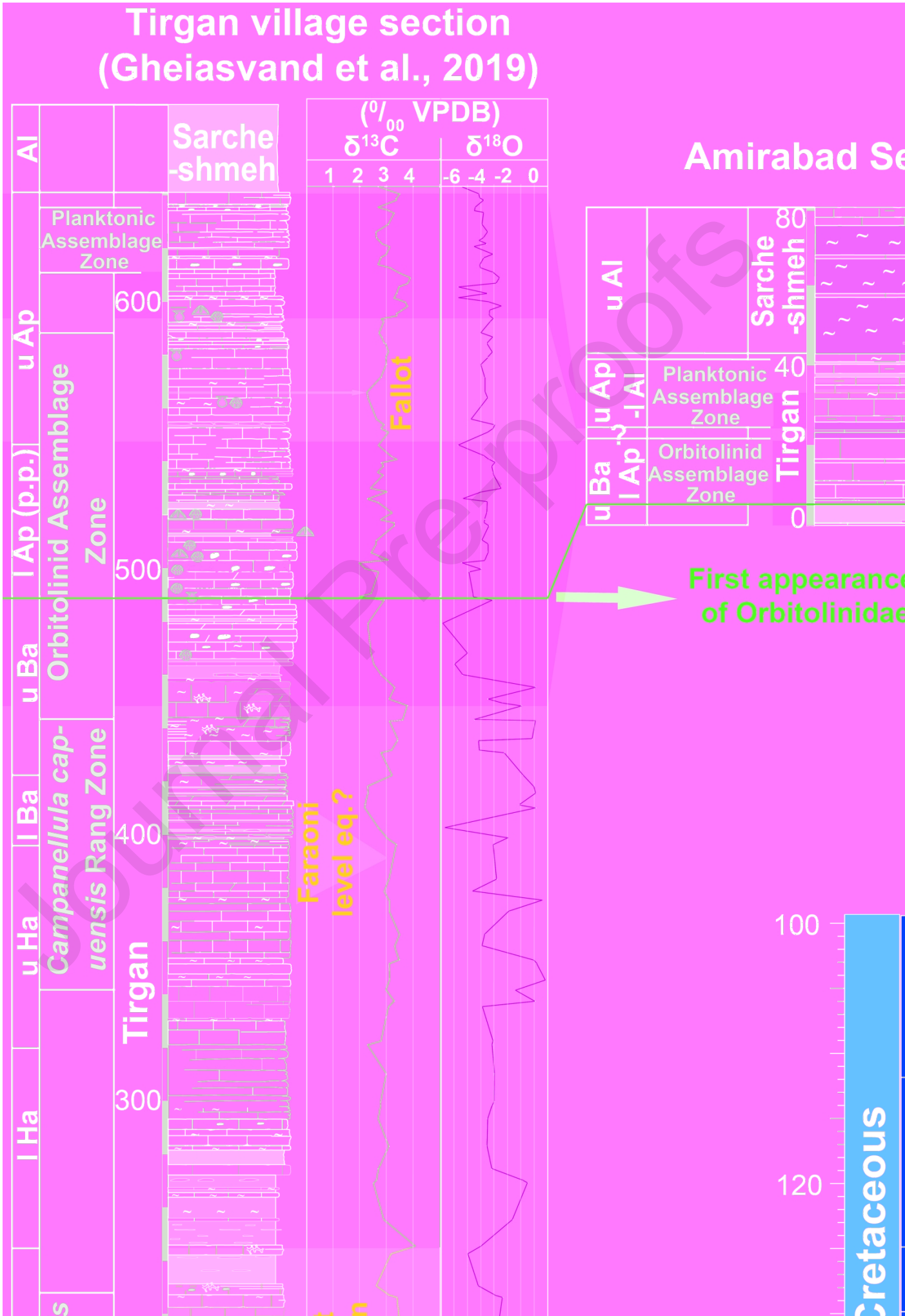
Tirgan village section
(Gheiasvand et al., 2019)
(‰ VPDB)
δ13C
δ18O
1 2 3 4
-6 -4 -2 0
Sarche-shmeh
Al
u Ap
l Ap (p.p.)
Planktonic Assemblage Zone
Orbitolinid Assemblage Zone
u Ba
l Ba
u Ha
l Ha
Campanellula cap-uensis Rang Zone
Tirgan
600
500
400
300
Fallot
Faraoni level eq.?
Amirabad Se
u Al
Sarche-shmeh
u Ap-l Al
Planktonic Assemblage Zone
u Ba-l Ap
Orbitolinid Assemblage Zone
Tirgan
80
40
0
First appearance of Orbitolinidae
100
120
Cretaceous

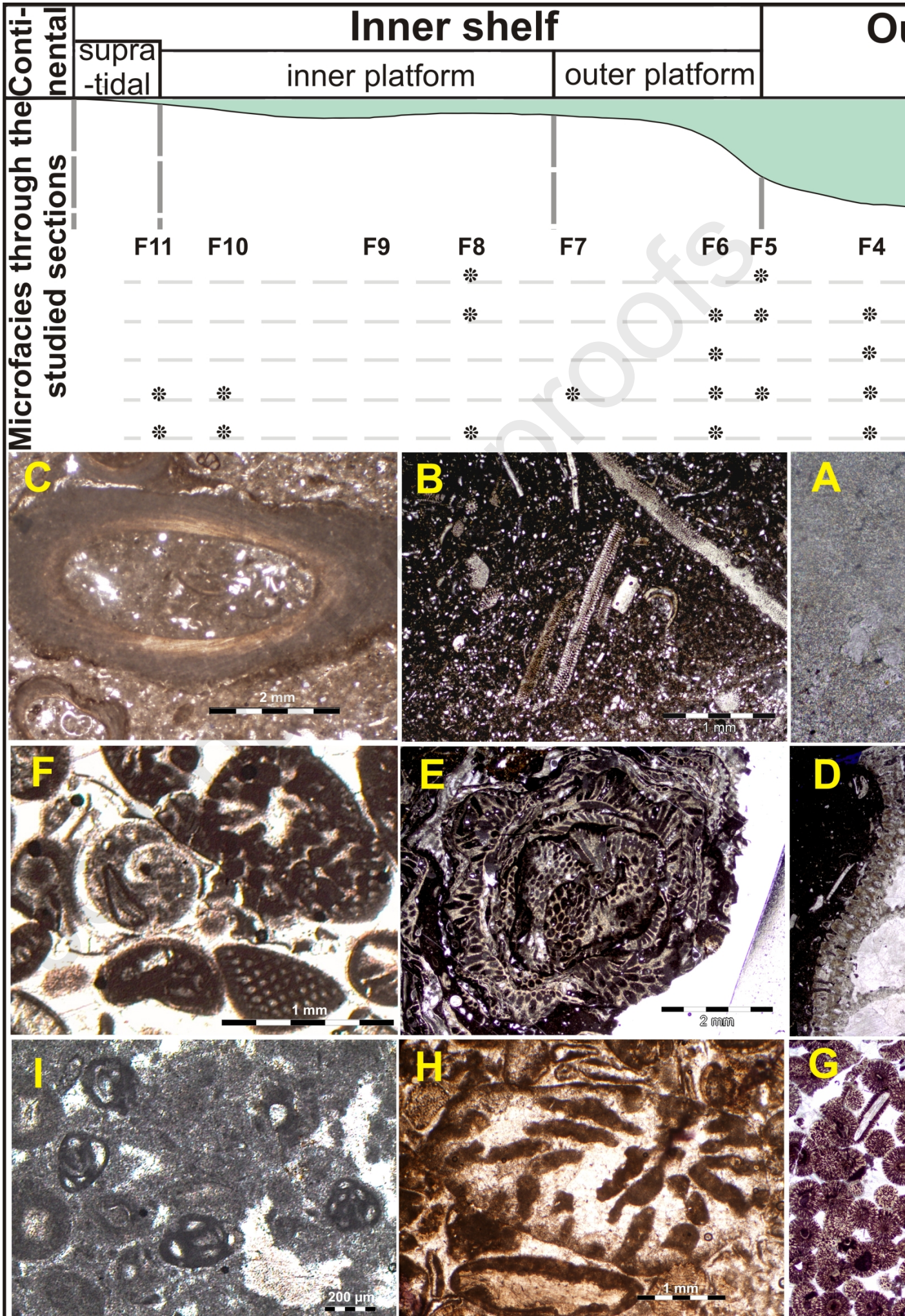
Conti-
nental
Inner shelf
supra
-tidal
inner platform
outer platform
Ou
Microfacies through the
studied sections
F11
F10
F9
F8
F7
F6
F5
F4
C
2 mm
B
1 mm
A
F
1 mm
E
2 mm
D
I
200 µm
H
1 mm
G

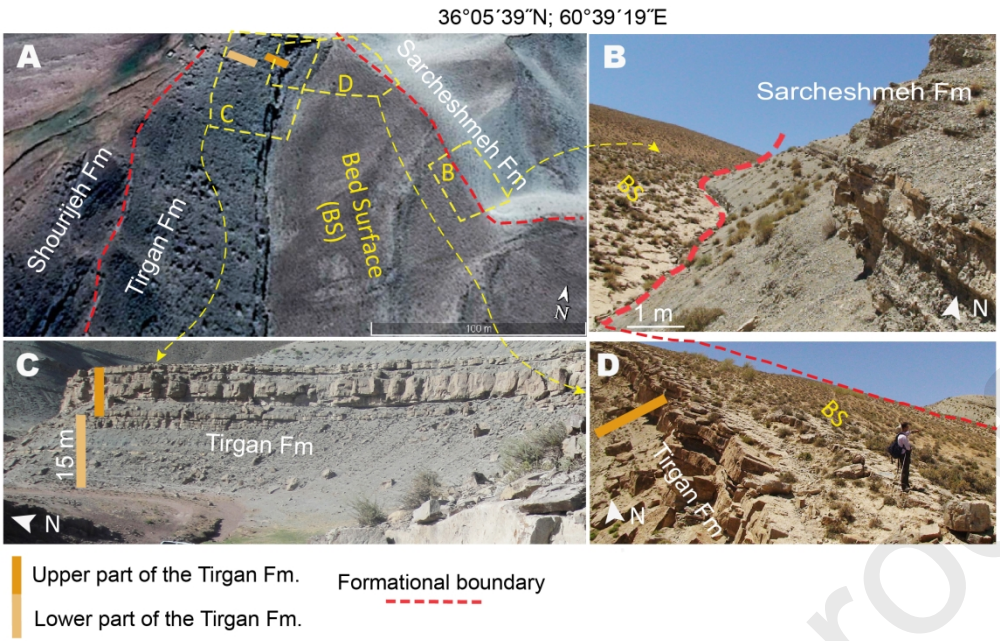

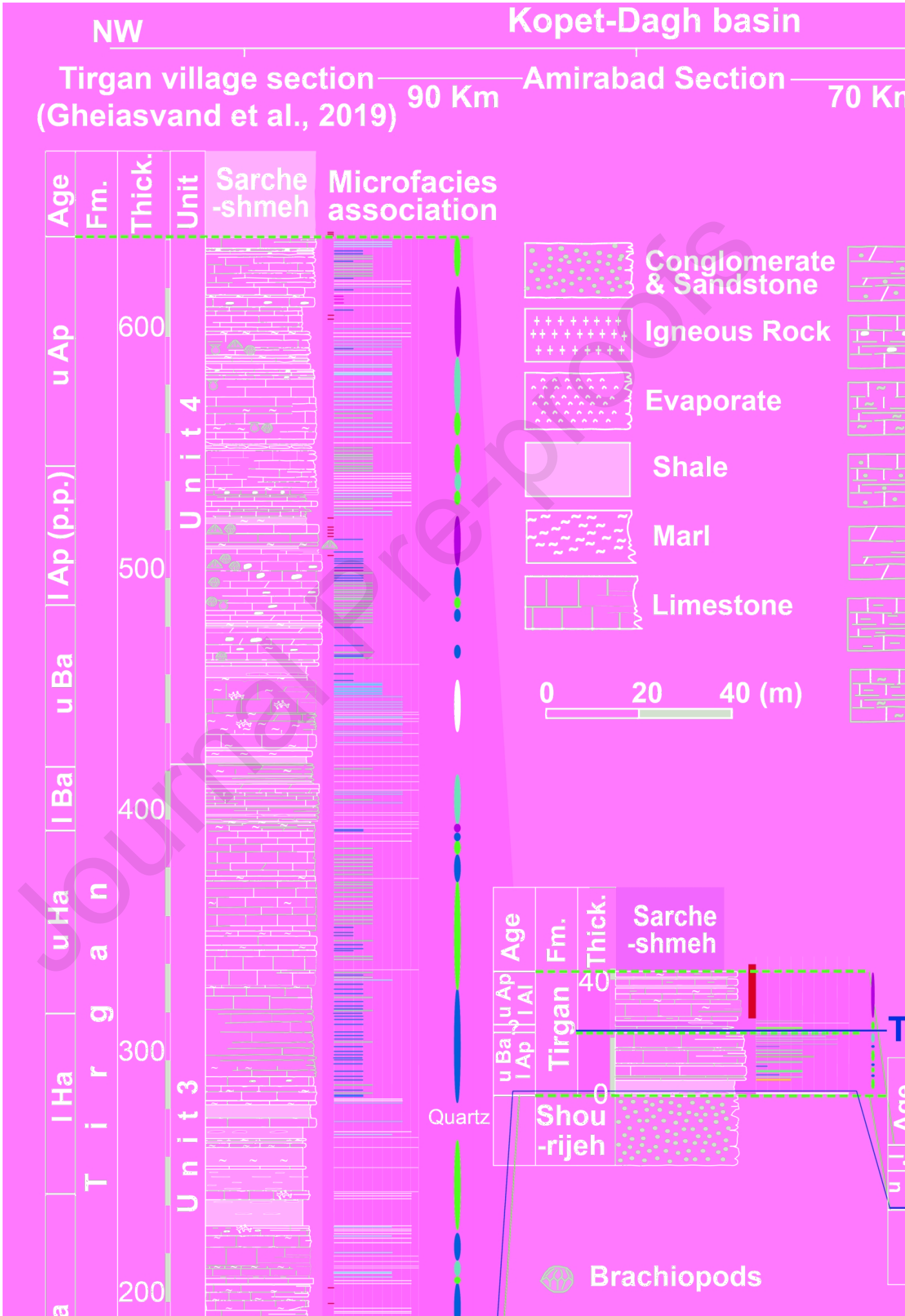
NW
Kopet-Dagh basin
Tirgan village section
(Gheiasvand et al., 2019)
90 Km
Amirabad Section
70 Km
Age
Fm.
Thick.
Unit
Sarche
-shmeh
Microfacies
association
u Ap
l Ap (p.p.)
u Ba
l Ba
u Ha
l Ha
Tirgan
Unit 4
Unit 3
600
500
400
300
200
Quartz
Conglomerate
& Sandstone
Igneous Rock
Evaporate
Shale
Marl
Limestone
0
20
40 (m)
l Ap
Tirgan
Shou
-rijeh
40
0
Brachiopods

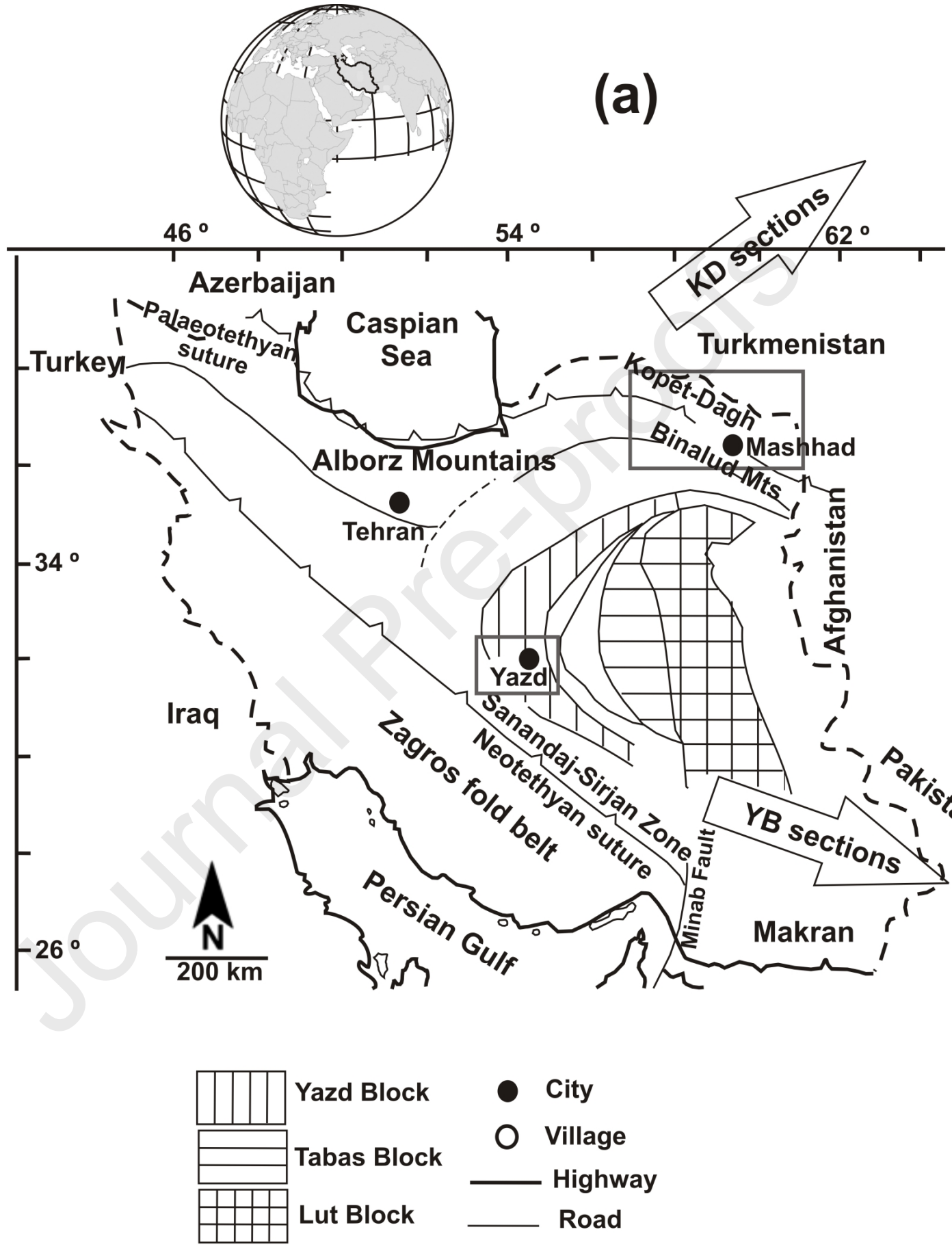

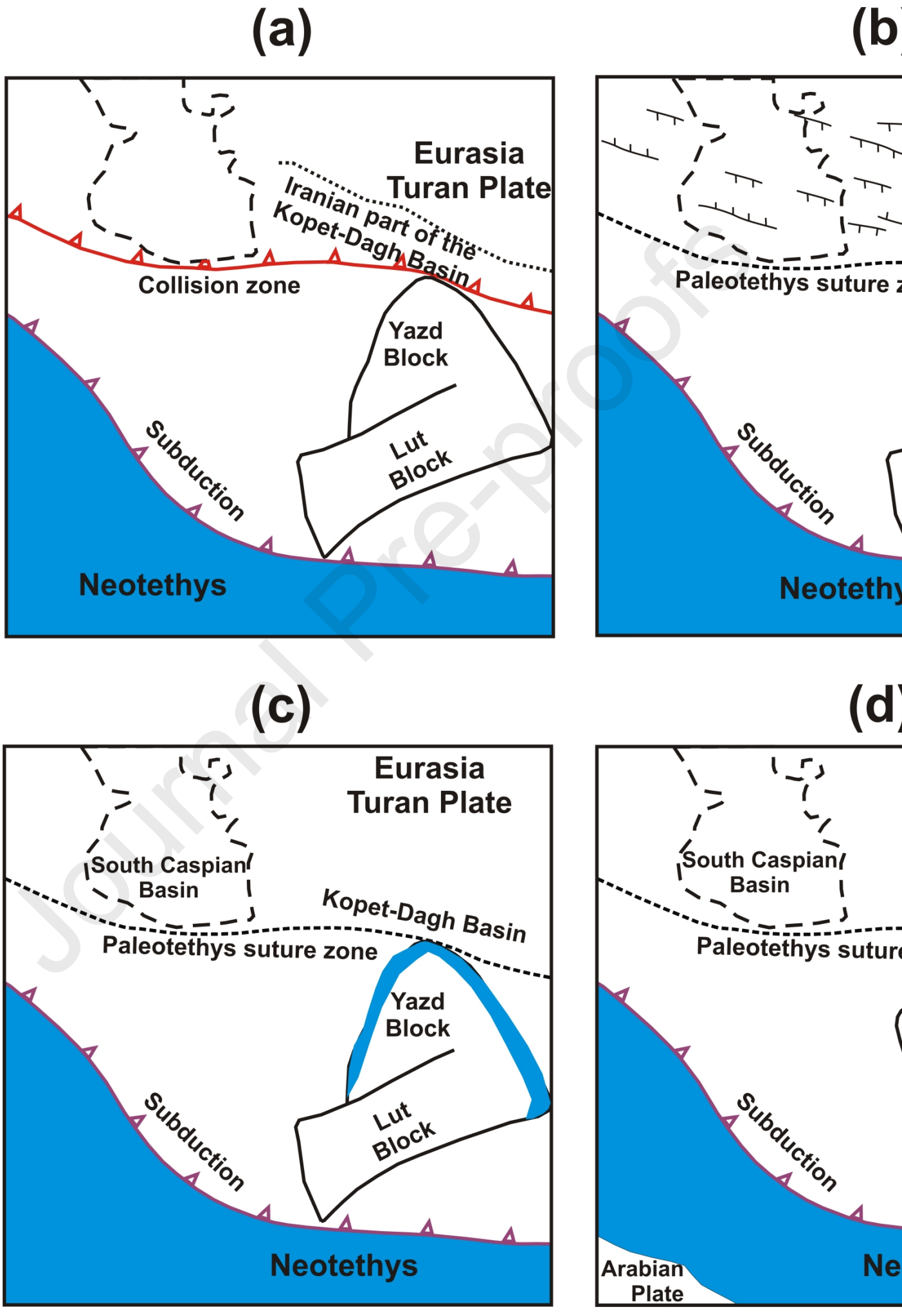

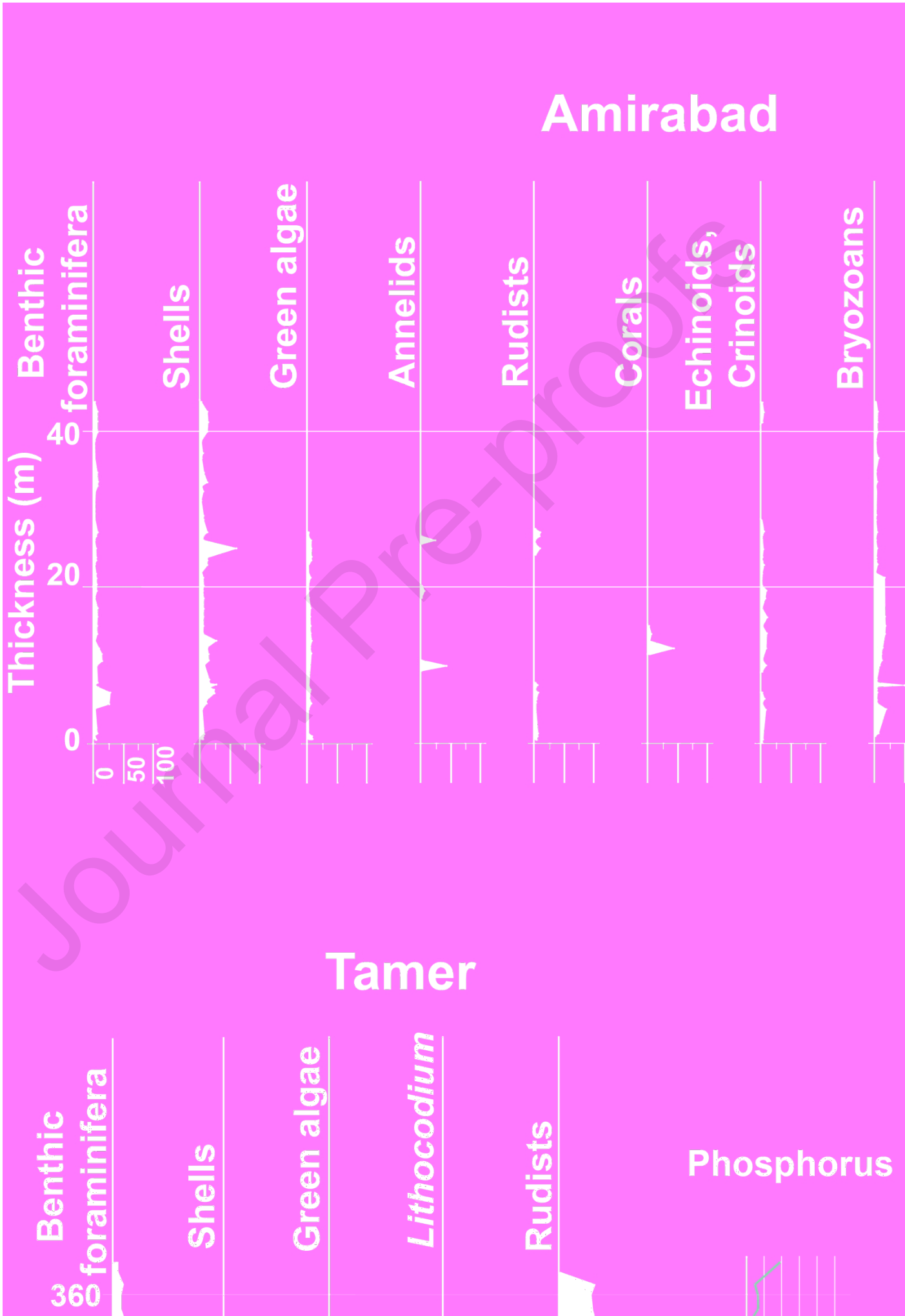

Association of microfacies	Short description	Environment
F1	Marly limestone and marl with less than 50% deeper marine organisms (e.g., calcispherids, radiolarian and colomiellids).	Outer-shelf (MF1)
F2	Marly limestone to wackestone, enriched in thin echinoid fragments.	Outer-shelf (MF1)
F3	Marly limestone to packstone and grainstone, together with small grains, dominant circalittoral foraminifera, including F3a; with abundant annelids.	Outer-shelf (MF1)
F4	Packstone, enriched in crinoids, calcareous sponges and bryozoans.	Outer-shelf (MF1)
F5	Grainstone, well-sorted and with large rounded fragments, consisting mainly of bioclastic accumulation.	Outer-platform (MF2)
F6	Oolitic facies.	Outer-platform (MF2)
F7	Grainstone made up of coral reef debris.	Outer-platform (MF2)
F8	Lagoonal facies; packstone to wackestone with abundant miliolids.	Inner-platform (MF3)
F10	Lagoonal facies; wackestone with abundant oncolites, indicating intense microbial activity.	Inner-platform (MF3)
F11	Supralittoral facies; including F11a; beach environment with keystone vugs and grainstone and F11b; muddy environment with algal mats, mudstone, bird's eyes and sheet cracks.	Supratidal

Geological setting	Section	Biozone	Identified microfossil	Thickness (m)	Age	Reference

Kopet-Dagh basin	Tirgan village	*Feurtillia gracilis* range zone	*Balkhania* sp., Calpionellids, *Danubiella* sp., *Epistomina* sp., ***Feurtillia gracilis***, *Haplophragmoides joukovskyi*, *Montsalevia salevensis*, *Scythiolina crumenaeformae*	138 to 230	l Va	All of the biozones through the Tirgan village section are after Gheiasvand et al., 2019
		Campanellula capuensis range zone	***Campanellula capuensis***, *Cuneolina camposaurii*, *Trocholina molesta*	342 to 442	l Ha-Ba	
		Orbitolinid assemblage zone	*Ammodiscus* cf. *glabratus*, *Balkhania* cf. *balkhanica*, *Cuneolina* sp., *Debarina hahounerensis*, ***« Dictyoconus » pachymarginalis***, *Dictyopsella* sp., *Gaudryna* sp., *Hensonina* sp., *Iraqia* cf. *hensoni*, *Meandrospira favrei*, *Montseciella* sp., *Neotrocholina friburgensis, N. sabbati*, *Patellina* sp., *Praeorbitolina*? *P. transiens*?, *Pseudocyclammina hedbergi*, ***Rectodictyoconus giganteus***, *Simplorbitolina* sp., *Valserina* sp.?, Undet. orbitolinid	487 to 587	e Ap-l Ap	
		Planktonic assemblage zone	*Arenobulimina* sp., calcispherids, colomiellids, ***Colomiella* sp.**, *Fisherina carinata, Gaudryina tuchaensis, Mesorbitolina* sp., *Novalesia cornucopia, Pseudotextulariella* sp., radiolarian, *Reticulinella reicheli*, *Verneuilina* aff. *Pharaonica*	610 to 635	l Ap	
	Amirabad	Orbitolinid assemblage zone	*Conorbinella azerbaidjanica*, ***Orbitolinopsis* cf. *nikolovi***, *Paleodictyoconus* sp., *Planispirilina* cf. *ranzenbergensis*, *Sabaudia briacensis*, *Trocholina molesta*, Undet. orbitolinid	5 to 22	e Ap	Gheiasvand et al., 2018
		Planktonic assemblage zone	*Cadosina* sp., calcispherids, colomiellids, ***Colomiella mexicana***, ***Colomiella* sp.**, ***Hedbergella* sp.**, radiolarian	24 to 40	l Ap-Al	This work
	Padeha	Orbitolinid assemblage zone	***« Dictyoconus » pachymarginalis*, *Kopetdagaria sphaerica***, Undet. orbitolinid	15 upwards	l Ba?-Ap	This work
Yazd Block	Tamer	Assemblage 1	*Bolivinopsis labeosa*, ***Cuneolina tenuis***, *C. camposaurii*, ***Decussoloculina barbui***, *Istriloculina eliptica*, *Quinqueloculina robusta*, *Trocholina molesta*, *Vercorsella* sp.	0 to 85	Va?-Ha	Both of the biozones through the Tamer section are after Gheiasvand et al., 2020
		Assemblage 2	***Arenobulimina chochleat***, *Belorussiella* cf. *taurica*, *Bolivinopsis labeosa*, *Charentia cuvillieri*, *Derventina filipescui*, ***« Dictyoconus » pachymarginalis***, *Everticyclammina* sp., *Glomospira urgoniana*, *Haplophragmoides* cf. *globosus*, *Istriloculina eliptica*, ***Martinotiella jucunda***, *Mayncina bulgarica*, *Novalesia cornucopia*, *Quinqueloculina robusta*, *Rumanoloculina* sp., ***Sabaudia minuta***, *S. briacensis*, *Trochamminoides coronus*, ***Vercorsella* aff. *immaturata***, *V. scarsellai*, *Vercorsella* sp.	85 to 345	l Ba-l Ap	
	Tehr	Assemblage 1	***Balkhania balkhanica***, *Charentia cuvillieri*, *Derventina filipescui*, ***« Dictyoconus » pachymarginalis***, *Iraqia simplex*?, *Istriloculina eliptica*, *Lenticulina* sp., *Nautiloculina bronnimanni*, *Orbitolinopsis* sp.?, ***Palorbitolina lenticularis***, *Palorbitolina* sp., *Pseudocyclammina* sp., *P. hedbergi*, *Quinqueloculina robusta*, *Vercorsella scarsellai*	0 to about 350	l Ba-e Ap	Both of the biozones through the Tehr section are after Gheiasvand et al., 2020
		Assemblage 2	*Arenobulimina cochleata*, *A. meltae*, *Charentia cuvillieri*, *Derventina filipescui*, *Lenticulina* sp., ***Mesorbitolina parva***, *Nautiloculina bronnimanni*, *Novalesia sp.*, *Orbitolinopsis* sp.?, *Paleodictyoconus* sp., *Palorbitolina* sp., *Praeorbitolina cormyi*, *P. claveli*, *Pseudocyclammina hedbergi*, *Quinqueloculina robusta*, ***Simplorbitolina manasi*** and *Valvulineria* sp.	360 to 590	l Ap	

Microfossil	Paleogeographic cluster	Locality	Tectonic element	paleoLat°/paleoLong°	Age	Reference
Decussoloculina barbui						
D.barbui	Northern Neotethys	Taft, Iran	Yazd	25.029381/ 75.358063	Va?-Ha	Gheiasvand et al., 2020
D.barbui	Southern Alpine Tethys	Crimea Mts.	Crimea	33.578769/ 55.511754	mid-Tithonian-Va	Krajewski and Olszewska, 2007
D.barbui	Southern Alpine Tethys	Crimea Mts.	Crimea	33.515134/ 55.428914	mid-Tithonian-Va	Krajewski and Olszewska, 2007

D.barbui	Southern Alpine Tethys	South Dobrogea, Romania	South Dobrogea	33.911905/ 49.664841	l Be-e Va	Dragastan et al., 2014

Microfossil	Paleogeographic cluster	Locality	Tectonic element	paleoLat°/paleoLong°	Age	Reference
Feurtillia gracilis						
F.gracilis	Northern Neotethys	Tirgan village, Iran	Aghdarband	29.433327/ 77.126902	l Va	Gheiasvand et al., 2019
F.gracilis	Southern Alpine Tethys	Cernavoda, Romania	South Dobrogea	37.877966/ 46.340047	l Be-Va	Neagu and Cîrnaru, 2002
F.gracilis	Southern Alpine Tethys	Bank of the Vederoasa lake, Romania	South Dobrogea	37.757464/ 46.178782	l Be-Va	Neagu and Cîrnaru, 2002
Bolivinopsis labeosa						
B.labeosa	Northern Neotethys	Taft, Iran	Yazd	29.794232/ 73.416997	Va?-Ha	Gheiasvand et al., 2020
B.labeosa	Southern Alpine Tethys	Muran Mts, Slovakia	West Carpathian	35.911159/ 34.903747	l Ha-e Ba	Lesná, 1997
Campanellula capuensis						
C.capuensis	Mid-Northern Pacific	Hole 866A	M1_MidPacific Plain	19.881112/ -87.098408	Ha, l Ha?	Arnaud-Vanneau and Silter, 1995
C.capuensis	Southern Neotethys	Zagros FTB, Iran	Ar Rayn	-4.739373/ 54.828254	Ha	Hosseini, 2014
C.capuensis	Northern Neotethys	Tirgan village, Iran	Aghdarband	29.433327/ 77.126902	l Ha-Ba	Gheiasvand et al., 2019
C.capuensis	Southern Alpine Tethys	Slovenia	Carnic Alps – South Karawanken	32.755366/ 35.038688	l Ha	Arnaud-Vanneau and Silter, 1995
C.capuensis	Southern Alpine Tethys	Mljet Island, Croatia	Karst	25.39486/ 32.578736	Ha-Ba	Husinec and Sokac, 2006
C.capuensis	Southern Neotethys	Fara San Martino, Italy	Apennine foredeep	22.60933/ 28.727924	Be-Ba	Bruni et al., 2007
C.capuensis	Southern Alpine Tethys	Adriatic platform	Central Bosnian	26.689123/ 32.626611	l Ha-Ba	Velić, 2007
C.capuensis	Southern Neotethys	Gafsa, Tunisia	Pelagia	18.328293/ 23.165672	Ha-Ba	Tawadros, 2011
C.capuensis	Southern Neotethys	Algeria	Iforas	16.123964/ 14.219171	Va-Ba	Loeblich and Tappan, 1988
C.capuensis	Northern Alpine Tethys	South Spain	East Central Iberian	33.254676/ 15.273894	l Ha	Arnaud-Vanneau and Silter, 1995

Microfossil	Paleogeographic cluster	Locality	Tectonic element	paleoLat°/paleoLong	Age	Reference
Conorbinella azerbaidjanica						
C.azerbaidjanica	Northern Neotethys	Gojgi village, Iran	Aghdarband	32.63376/ 78.08652	e Ap	Gheiasvand et al., 2018
C.azerbaidjanica	Northern Neotethys	Azerbaidjan	Kura	37.365919/ 65.359531	l Ba-l Ap	Poroshina, 1976
C.azerbaidjanica	Northern Alpine Tethys	France	Ligerian	43.818584/ 20.876863	l Ba-l Ap	Loeblich and Tappan, 1988
Orbitolinopsis nikolovi						
O.nikolovi	Northern Neotethys	Gojgi village, Iran	Aghdarband	32.633759/ 78.086519	e Ap	Gheiasvand et al., 2018
O.nikolovi	Southern Alpine Tethys	Bogovina, Serbia	South Getic	39.851227/ 37.402578	l Ba-e Ap	Sudar et al., 2008
O.nikolovi	Southern Neotethys	Northern Chotts chain, Tunisia	Aïr	19.725975/ 22.281629	e Ap	Hfaiedh et al., 2013
Arenobulimina cochleata						
A.cochleata	Northern Neotethys	Taft, Iran	Yazd	32.177054/ 72.211846	Ap	Gheiasvand et al., 2020
A.cochleata	Northern Neotethys	Taft, Iran	Yazd	32.386969/ 72.058509	l Ba, Ap	Gheiasvand et al., 2020
A.cochleata	Southern Neotethys	Oman	Semail	-7.197054/ 58.043594	e Ap	Chartrousse and Masse, 1998
A.cochleata	Southern Alpine Tethys	Dobrogea, Romania	South Dobrogea	40.789749/ 44.533557	e Ba-Ap	Neagu, 1997
A.cochleata	Northern Alpine Tethys	Switzerland	PreAlps Briançonnais	36.966771/ 25.386239	e Ap	Arnaud-Vanneau and Silter, 1995
A.cochleata	Northern Alpine Tethys	Vercors	Chamrousse	42.286823/ 24.315788	e Ap	Arnaud-Vanneau and Silter, 1995
A.cochleata	Northern Alpine Tethys	Spain	East Central Iberian	36.357241/ 14.272595	e Ap	Arnaud-Vanneau and Silter, 1995
Colomiella sp.						
C.sp	Northern Neotethys	Tirgan village, Iran	Aghdarband	33.084987/ 77.267543	l Ap	Gheiasvand et al., 2019
C.sp	Northern Neotethys	Gojgi village, Iran	Aghdarband	32.633759/ 78.086519	l Ap-Al	This work
C.sp	Southern Neotethys	J. Mrhila, Tunisia	Pelagia	20.847819/ 22.945673	l Ap	Zghal et al., 1996
C.sp	Gulf of Mexico	Tamaulipas, Mexico	Guachichil	24.076056/ -46.815259	l Ap-e Al	Longoria and Gamper, 1974
C.sp	Gulf of Mexico	Mexico	Caborca	30.968949/ -55.265930	l Ap-Al	Trejo, 1975
C.sp	East-Northern Pacific	La Pena, Mexico	Teloloapan	15.364651/ -60.275043	l Ap-e Al	Longoria, 1972
Arenobulimina meltae						
A.meltae	Northern Neotethys	Taft, Iran	Yazd	32.386969/ 72.058509	Ap	Gheiasvand et al., 2020
A.meltae	Southern Alpine Tethys	Bulgaria	Moesia	39.099468/ 41.464653	l Ba, Ap	Kovatcheva, 1979
Martinotiella jucunda						
M.jucunda	Northern Neotethys	Taft, Iran	Yazd	32.177054/ 72.211846	Ap	Gheiasvand et al., 2020
M.jucunda	Northern Alpine Tethys	Bajuvaric, Austria	Helvetic	44.975957/ 32.196307	e Ap-Al	Rehakova et al., 1996

Mayncina bulgarica						
M.bulgarica	Northern Neotethys	Taft, Iran	Yazd	32.177054/ 72.211846	Ap	Gheiasvand et al., 2020
M.bulgarica	Northern Neotethys	Lesser Caucasus	Sanandaj	33.817497/ 50.551756	Ap	Voznesenskii et al., 2002
M.bulgarica	Southern Alpine Tethys	Mljet Island, Croatia	Karst	27.665772/ 31.269038	Ha-e Al	Husinec and Sokac, 2006
Simplorbitolina manasi						
S.manasi	Northern Neotethys	Chenaran, Iran	Aghdarband	32.777605/ 77.069458	Ap	Yavarmanesh et al., 2017
S.manasi	Northern Neotethys	Taft, Iran	Yazd	32.386969/ 72.058509	l Ap	Gheiasvand et al., 2020
S.manasi	Southern Neotethys	Shiraz, Iran	Ar Rayn	0.854202/ 54.775216	l Ap	Afghah and Fanati Rashidi, 2007
S.manasi	Southern Alpine Tethys	Transdanubia, Hungary	Transdanubian	35.762954/ 34.854946	l Ap	Bodrogi, 1999
S.manasi	Northern Alpine Tethys	Spain	Cantabria	39.396972/ 15.425611	l Ap-Al	Schlagintweit et al., 2016

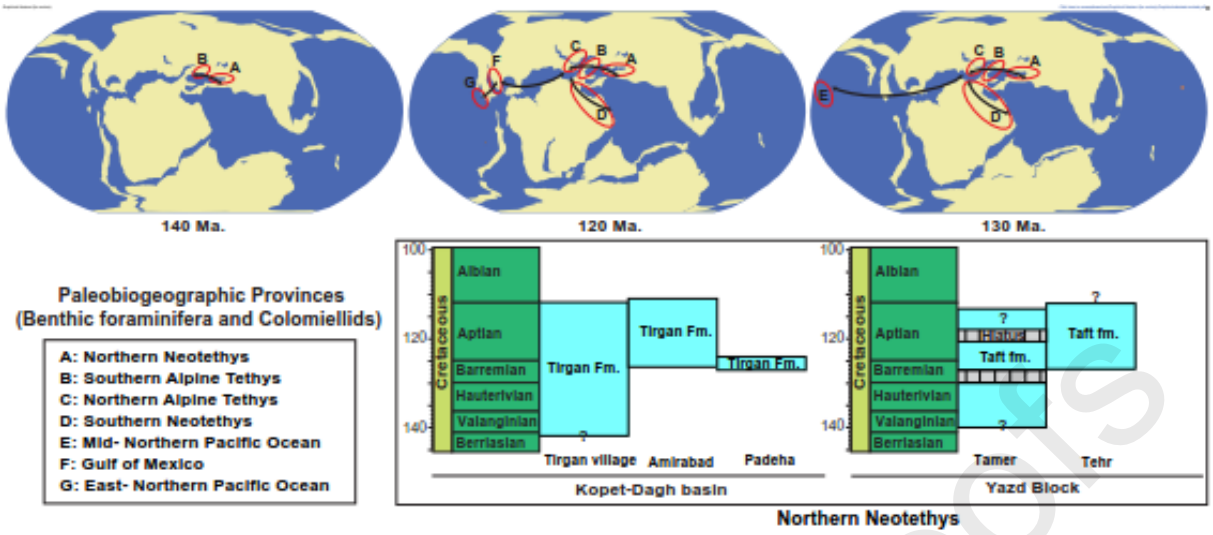

Highlights

- The Early Cretaceous biozone ages in NE and Central Iran were refined by δ ^{13}C trend.
- Paleobiogeographic provinces of foraminifera and colomiellids were worldwide defined.
- Diachrony of studied deposits reflects subsidence effects and remnant paleoreliefs.
- P content in the deposits shows changes from photozoan to heterozoan assemblages.
- The deposits indicate environmental changes similar to those in other Tethyan realms.

We the undersigned declare that this manuscript is original, has not been published before and is not currently being considered for publication elsewhere.

We confirm that the manuscript has been read and approved by all named authors and that there are no other persons who satisfied the criteria for authorship but are not listed. We further confirm that the order of authors listed in the manuscript has been approved by all of us.

We understand that the Corresponding Author is the sole contact for the Editorial process. He/she is responsible for communicating with the other authors about progress, submissions of revisions and final approval of proofs.

Signed by the corresponding author:

Masoumeh Gheiasvand

Ferdowsi University of Mashhad

Masoumeh Gheiasvand: Conceptualization, Investigation, Methodology, Software, Formal analysis, Visualization, Writing- original draft, review and editing, **Karl B. Föllmi:** Resources, Validation, Investigation, Data curation, **Gérard M. Stampfli:** Supervision, Validation, Data curation, Writing- review and editing, **Christian Vérard*:*** Methodology, Software, Formal analysis, Writing- review and editing, **Michele Morsilli:** Methodology, Writing- review and editing, **Valeria Luciani:** Writing- review and editing